https://doi.org/10.5194/egusphere-2026-3058
Preprint. Discussion started: 24 June 2026


# Cryogenic Fractionation and Thaw-Gradient Reorganization of Carbon, Nutrient and Trace Element Pools in Permafrost Peatlands

Lucia Pérez-Serrano[1,2], Sergey V. Loiko[3], Artem Lim[3], Laure Gandois[2], Christine Hatté[4,5], Jean-Luc Rols[2], and Oleg S. Pokrovsky[1].

[1] Géosciences Environnement Toulouse, Université de Toulouse, Toulouse, France
[2] Centre de Recherche sur le Biodiversité et l'Environnement, Université de Toulouse, CNRS, IRD, Toulouse, France
[3] BIO-GEO-CLIM Laboratory, Tomsk State University, Tomsk, Russia
[4] Laboratoire des Sciences du Climat et de l'Environnement, LSCE/IPSL, UMR 8212, CEA CNRS UVSQ, Université Paris-Saclay, 91191 Gif-sur-Yvette, France
[5] Institute of Physics, Silesian University of Technology, 44-100 Gliwice, Poland

*Correspondence to*: Lucia Pérez-Serrano (lucia.perez-serrano@utoulouse.fr)

**Abstract**

Permafrost peatlands are highly vulnerable to climate warming because active layer deepening can mobilize previously frozen solutes into suprapermafrost flow paths and regional hydrological networks. Yet the composition of the frozen porewater reservoir, i.e., pore ice, and its role in regulating C, nutrient and trace-element release during thaw, remain poorly constrained. Here, we characterized dissolved organic matter (DOM), nutrients, and major and trace solutes across the active layer–permafrost interface in a continuous (> 90 % ice) polygonal peatland of the subarctic tundra. Four microtopes representing a thaw gradient (convex polygon → concave polygon→ peat transitional fen → peat-mineral fen) were sampled, with porewater and pore ice (< 0.45 µm) analyzed in active and frozen layers. Pore ice DOM showed a predominantly microbial and aliphatic signature, with elevated dissolved organic carbon (DOC) concentrations, indicating selective preservation of microbially processed, low-aromatic compounds during freezing. Freeze–thaw cycling homogenized active layer porewater chemistry, whereas pore ice retained stronger site-specific geochemical signatures. Overall, DOC, dissolved N and P, and exchangeable cations (Ca, Mn, Ba, Sr) preferentially accumulated in pore ice, while lithogenic elements (Zr, Ga, Hf, Ge, Nb, Cr, Y and REE) were more concentrated in active layer porewaters. Frozen horizons also exhibited lower C:N:P ratios than active layers, highlighting nutrient-enriched stoichiometry in the permafrost compartment. A coupled stoichiometric and decay-rate model suggests that phosphorus is largely consumed *in situ* during progressive thaw, thereby constraining further carbon and nitrogen processing, whereas substantial fractions of DOC and dissolved N remain available for lateral export. Viewed as a space-for-time thaw sequence, the transition from polygonal bog to fen indicates that permafrost degradation may initially enhance mobilization of labile carbon and nutrients before hydrological redistribution dominates. These results identify pore ice as both

https://doi.org/10.5194/egusphere-2026-3058
Preprint. Discussion started: 24 June 2026


a cryogenic archive of past biogeochemical processing and a reactive reservoir capable of amplifying Arctic carbon–nutrient fluxes under continued warming.

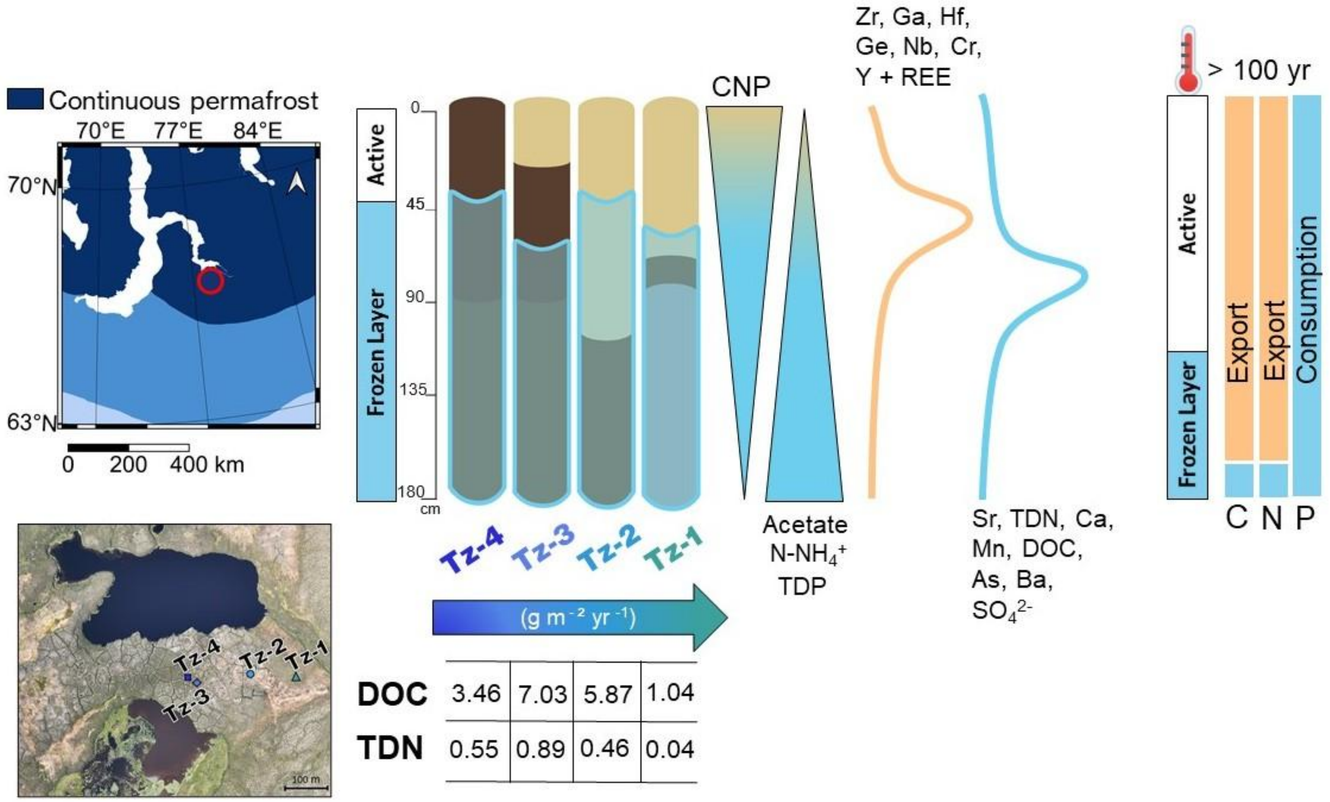


## 1 Introduction

Northern permafrost peatlands play a major role in the climate system, exerting a net cooling effect on the global radiation balance through sequestration of atmospheric carbon over millennia. As the Arctic has warmed nearly four times the rate of the global average the last four decades (Rantanen et al., 2022), destabilization of the sequestered C (185 ± 66 Pg C, (Hugelius et al., 2020) through emissions from inland water surfaces and export to major river systems is likely to occur (Frey and Smith, 2005). One of the largest frozen peatland provinces in the world is the Western Siberia Lowland (WSL), which holds 1.05 million km$^2$ permafrost-bearing soils, with an estimated peatland coverage of 592.440 km$^2$ and a total C pool of 70.21 Pg C (Sheng et al., 2004). High vulnerability of the frozen peat is linked to its average temperature slightly below 0 °C (Romanovsky et al., 2010; Raudina et al., 2025a). Climate warming may retreat the permafrost boundary to northern latitudes (Frey et al., 2007; Sherstyukov and Sherstyukov, 2015; Fewster et al., 2023), which implies an increase in the area of negative forms of relief (hollows and subsidences) compared to the positive ones (mounds and polygons) (Pastukhov et al., 2017) and a deepening of the active layer thickness (Åkerman and Johansson, 2008; Romanovsky et al., 2010). The active layer undergoes seasonal thawing-freezing and is responsible for water transport along the permafrost table (Woo, 2012; Liao and Zhuang, 2017; Koch et al., 2024). This suprapermafrost flow is the main source of incoming solutes to thermokarst lakes during summer periods, and a complementary source for rivers in WSL (Raudina et al., 2017a; Krickov et al., 2026).

Solutes from permafrost soils are rich in dissolved organic carbon (DOC), macro and micro-nutrients, and toxicants, especially if issued from the peat layer (Kuzmina et al., 2023). Peat organic soil is a highly complex porous medium which host variable ground ice structures in terms of size and time scale (Fu et al., 2022), and thawing of pore ice can result in the opening of isolated (non-connected) pores that contain solutes and bacteria (Morgalev et al., 2023). Besides, thawing of the permanent frozen layer may alter hydrological pathways, which will also come with a mobilization of unaccounted dissolved organic matter (DOM) pools, resulting in an enrichment in DOC, nutrients and metals of aquatic ecosystems(Vonk et al., 2015; O'Donnell et al., 2024), which can significantly affect C, N and P cycling.

For all the permafrost zones in the Western Siberian Lowland, a strong local maximum of DOC, P, Ca, Fe and other trace elements concentration in pore ice was discovered below the current active layer boundary (Lim et al., 2021). Moreover, a sizable enrichment in the pore ice of the frozen layer relative to the pore water of the active layer is present for DOC, metal micro-nutrients and other DOM-bounded metals (Lim et al., 2021, 2022). Suprapermafrost flow in continuous permafrost zones (> 90 % ice) in the WSL showed higher concentrations of major cations (Ca, Mg), micro-nutrients (Cu), other metals (Ni, REE) and DOC compared to less ice-rich zones (Raudina et al., 2018). Assuming permafrost thaw scenarios with an active layer thickness (ALT) increase by 1 cm $yr^{-1}$ (Åkerman and Johansson, 2008), the export of labile C, nutrients (P) and metals (Zn) may at least double the annual delivery of WSL rivers to the Arctic Ocean (Lim et al., 2021).

While previous investigations in polygonal peatlands of the Western Siberian Lowland demonstrated substantial reservoirs of carbon, nutrients and trace elements stored below the contemporary active layer boundary, particularly within polygon uplands (Lim et al., 2021; Kuzmina et al., 2023), these studies largely emphasized bulk inventories and vertical contrasts between frozen and seasonally thawed layers. In contrast, how these reservoirs vary across microtopographic units representing different stages of thaw remains insufficiently resolved. In polygonal peatlands, bog mounds, troughs and fen systems form a natural thaw gradient associated with progressive subsidence, increasing hydrological connectivity and intensified suprapermafrost flow. Investigating porewater and pore ice chemistry along this microtope sequence (convex polygon → concave polygon → peat transitional fen → peat-mineral fen) therefore provides a space-for-time framework to evaluate how thaw-driven landscape transformation reorganizes DOM and nutrient storage, and how cryogenic solute partitioning evolves across this gradient.

Specifically, this study aims to: (i) quantify DOM concentration and composition in pore ice and active layer porewaters across contrasting microtopes; (ii) determine how position along the thaw gradient influences solute partitioning between frozen and thawed compartments; (iii) assess the relative storage of macro- (carbon, nitrogen and phosphorus) and micronutrients in pore ice *versus* active layer waters; and (iv) estimate the potential long-term remobilization of these reservoirs under projected active layer deepening. Particular attention is given to micro-landscape controls on pore ice formation and composition, as spatial position and hydrological residence time govern the capacity of suprapermafrost flow to mobilize and redistribute

https://doi.org/10.5194/egusphere-2026-3058
Preprint. Discussion started: 24 June 2026


bioavailable solutes within the peatland and toward the broader hydrological network. By integrating microtopographic variability with porewater–pore ice contrasts across a thaw gradient, this study advances from static reservoir assessment toward a predictive understanding of how permafrost peatlands may reorganize carbon and nutrient pools under continued warming, with implications for high-latitude carbon export and climate feedbacks.

## 2 Study site and methods

### 2.1. Geographical setting and soil-water ice sampling

Core samples (0–180 cm) were collected on August 2023 in Tazovsky site of the INTERACT stations of Western Siberia located in a flat polygonal peatland in the subarctic tundra (Fig. 1). The mean annual air temperature is -9.1 °C and the mean annual precipitation is 363 mm (Lim et al., 2021). Peat soil overlays a mineral substrate of clay loam and loam. Tz-1 (67.358425 °N, 78.711545 °E) was sampled at the peat-mineral fen (mineral layer > 80 cm depth), Tz-2 (67.35318 °N, 78.709593 °E) corresponds to the transitional fen, Tz-3 was sampled in a convex polygon (67.35752 °N, 78.706847 °E), and Tz-4 (67.35746 °N, 78.706267 °E) at a concave polygon. Shrub-lichen polygons configurate an ombrotrophic bog along with the interpolygonal depressions (troughs) dominated by grass dwarf-sphagnum (Pastukhov et al., 2022).Peat extends more than 2 m depth, with a variable degree of decomposition (Ombric Sapric → Hemic Muusic → Hemic Histosols) depending on the microsite position in the catena (Pastukhov et al., 2025).

One core was collected per microsite along the thaw gradient (polygonal bog, transitional fen, peat–mineral fen). Although no within-site replicates were obtained, this design is supported by previous multi-core investigations at the Tazovsky site demonstrating relatively low small-scale spatial variability within comparable geomorphological units (Loiko et al., 2019, 2023). Earlier surveys of independent cores from the region showed < 30 % variation in soluble organic carbon and consistent vertical trends in physical properties (bulk density, horizon structure) and major solute distributions. Across multiple mineral and peat soils, reproducible depth-dependent hydrochemical profiles indicated coherent pedogenic structure and comparable solute migration regimes within each microtopographic class (Lim et al., 2025a). Given this documented regional consistency, the selected cores are considered representative of their respective microsites in terms of vegetation, soil type, ground ice characteristics and active layer thickness. The primary objective of this study was to resolve vertical partitioning between active layer porewaters and underlying pore ice across distinct thaw stages, rather than to quantify lateral heterogeneity within a single microsite. Accordingly, analytical effort was concentrated on high-resolution intra-core profiling of DOM, nutrients and trace elements across the active layer–permafrost interface. While additional replication would further constrain microscale variability, the combination of previously established spatial coherence and detailed depth-resolved analyses provides a statistically defensible framework for evaluating thaw-gradient controls on porewater and pore ice chemistry. The design prioritizes process-level contrasts among microtopes over fine-scale within-site variability, consistent with established approaches in permafrost soil geochemistry.

https://doi.org/10.5194/egusphere-2026-3058
Preprint. Discussion started: 24 June 2026


For all cores, the active layer (AL) is situated in the peat soil. The AL thickness at the moment of sampling was 55 ± 5 cm for Tz-1, 40 ± 5 cm for Tz-2, 60 ± 5 cm for Tz-3, and 40 ± 5 cm for Tz-4. The cores (4 cm diameter) were extracted using a Russian peat borer following previous methodology in the area (Lim et al., 2021, 2022; Kuzmina et al., 2023), cut using a ceramic blade into 5-cm and 10-cm layers for horizons deeper than 100 cm, and thawed at room temperature. Immediately after full thawing of the frozen core, peat water was extracted through 100-µm pre-cleaned Nylon net by applying a local confining pressure (1–5 kg cm$^{-2}$, depending on sample humidity). The obtained slurry was centrifuged (15 min at 1096 *g*) and the supernatant was filtered through 0.45-µm acetate cellulose filter with the first 10 mL of filtrate discarded.

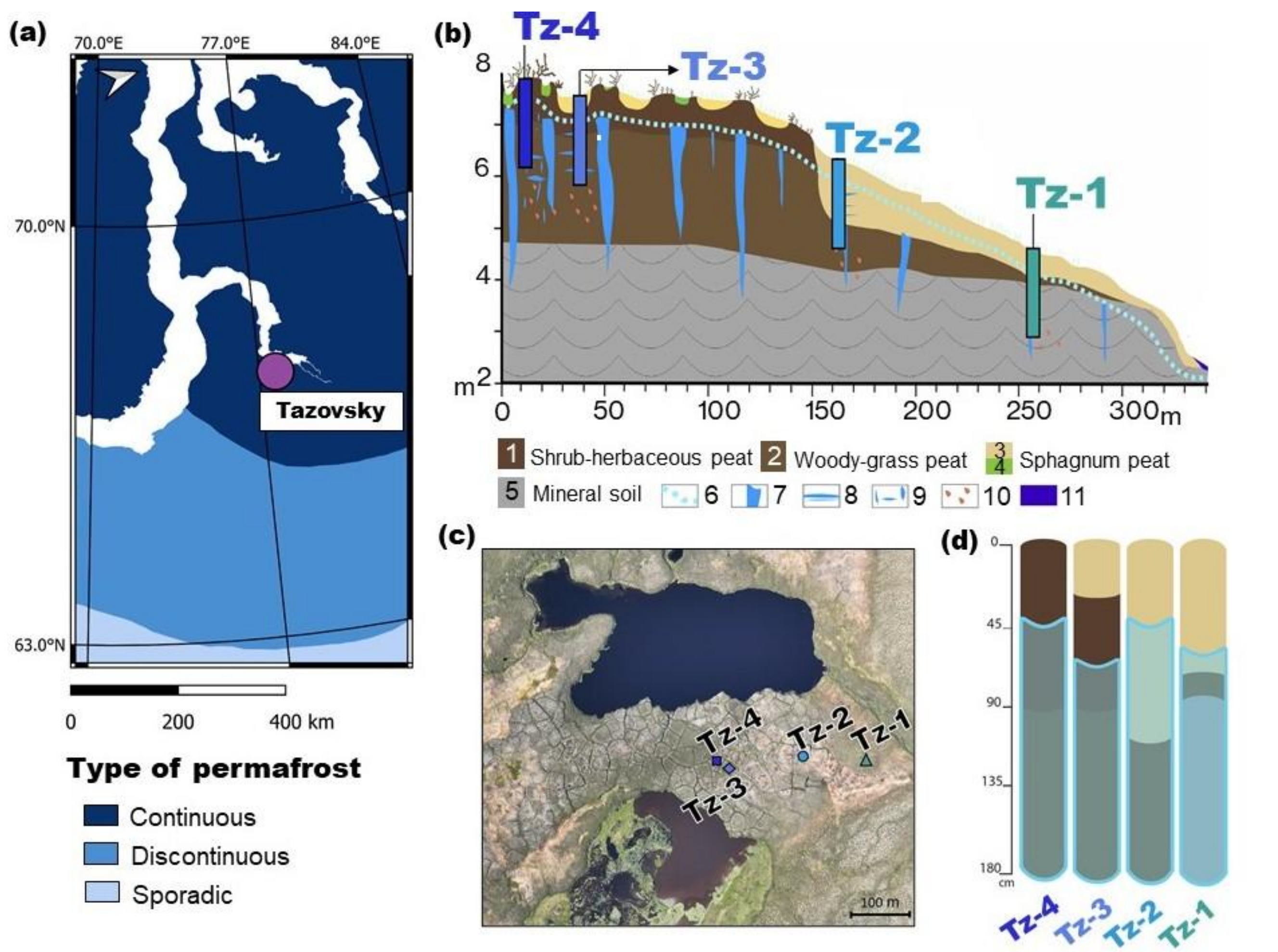


Figure 1. (a) Map of permafrost boundaries after Muster et al. (2017). (b) Profile section showing type of soil (1-5), cryogenic forms (6 – upper limit of permafrost; 7 – ice veins; 8 – layered cryo-texture; 9 – mesh cryotexture), soil texture (10 – remains of stems and branches) and stream (11). (c) Aerial view of Tazovsky sampling sites, and (d) depth of the active and frozen layers for sample cores at each site. Different microtopes labelled as Tz-4 to Tz-1 represent a thawing gradient of the polygonal peatland ecosystem (□, convex polygon → ◊, concave polygon → ○, peat transitional fen → Δ, peat-mineral fen).

https://doi.org/10.5194/egusphere-2026-3058
Preprint. Discussion started: 24 June 2026


### 2.2. Analyses

The filtered samples (< 0.45 µm) were divided in two fractions: (1) acidified (1% ultrapure double-distilled $HNO_3$) for trace elements analysis and (2) non-acidified for DOC, Total Dissolved N (TDN), cations, anions, and organic acids analysis. Major elements (Ca, Mg, Na, K, Si) along with 47 trace elements were determined with an Thermo iCap Triple Quad (TQ) ICP MS using both Ar and He modes to diminish the interferences. In and Re were added on-line as internal standard. The typical uncertainty for elemental concentration measurements ranged from 5 to 10 % at 1–1000 µg $L^{-1}$ to 10–20 % at 0.001–0.1 µg $L^{-1}$. The SLRS-6 (Riverine Water Reference Material for Trace Metals certified by the National Research Council of Canada) agreement between replicated measurements of SLRS-6 and the certified values (< 15 %) are reported in this study.

The pH was measured with an uncertainty of ± 0.02 pH units. Ultraviolet and visual absorbance of non-acidified filtered samples was measured between 200 and 800 nm using a 10-mm quartz cuvette on a Cary-50 spectrophotometer. $SUVA_{254}$ (L $mg^{-1}$ $m^{-1}$) was calculated after Weishaar et al., (2003) to assess the relative amount of aromatic C, then corrected as the mass iron (III):DOC concentration ratios (mg:g) were ≤ 0.35 (Poulin et al., 2014). Fluorescence was measured using a BioTek Synergy H1 Multimode microplate reader, and the Fluorescence index (FI) was calculated after McKnight et al. (2001), to distinguish between DOM derived from plants (FI < 1.4) and microbial origin (FI > 1.4) (Roehm et al., 2009; Cory et al., 2010).

DOC and TDN were analyzed using a Carbon Total Analyzer (Shimadzu TOC-L) with an uncertainty better than 3 % and a detection limit of 0.01 mg $L^{-1}$ and 0.1 mg $L^{-1}$, respectively. Nineteen organic acids were analyzed (glycolate, propionate, formate, butyrate, isobutyrate, pyruvate, glutarate, galacturonate, valerate, tartrate, malate, maleate, oxalate, fumarate, alpha-keto-glutarate, phthalate, citrate, lactate and acetate), along with main inorganic anions $F^-$, $Br^-$, $Cl^-$, $SO_4^{2-}$, N-$NO_2^-$, N-$NO_3^-$ and P-$PO_4^{3-}$, as well as cations $Ca^{2+}$, $Li^+$, $Na^+$, N-$NH_4^+$, $K^+$ and $Mg^{2+}$ by high-performance ionic chromatography (Dionex Ics-5000 and Dionex DX-120, respectively), both with an uncertainty of 2 %. Quantification limits were 0.001 mg $L^{-1}$ for $Li^+$, $F^-$, $Br^-$, P-$PO_4^{3-}$, and N-$NO_2^-$; 0.05 mg $L^{-1}$ for $Mg^{2+}$ and $Cl^-$; 0.01 mg $L^{-1}$ for $Na^+$, $K^+$, N-$NO_3^-$ and $SO_4^{2-}$ ; 0.03 mg $L^{-1}$ for N-$NH_4^+$ and 0.002 mg $L^{-1}$ for organic acids. Dissolved Organic Nitrogen (DON) is calculated as the difference of TDN minus the inorganic forms (for N-$NH_4^+$, N-$NO_2^-$, N-$NO_3^-$).

Soil samples from Tz-4 (n = 7), Tz-3 (n = 5), Tz-2 (n = 6) and Tz-1 (n = 3) were selected for $^{14}C$ dating using a Mini Carbon dating System (MICADAS) in the Laboratoire des Sciences du Climat et de l'Environnement (LSCE) (Hatté et al., 2024; Thil et al., 2024), and the Accelerator Mass Spectrometer (AMS) Artemis in the Laboratoire de Mesure du Carbone 14 (LMC14) (Moreau et al., 2013; Dumoulin et al., 2017). The radiocarbon dates were calibrated with IntCal20 atmospheric curve (Reimer et al., 2020). Age-depth models were calculated using the OxCal v4.4.4 software (Ramsey, 2001, 2008; Ramsey and Lee, 2013) with 2 cm resolution, and P_Sequence function with parameters $k_0 = 1$ and $\log_{10}(k/k_0) \in [-2,2]$ was applied. The peat accumulation rate (mm $yr^{-1}$) was calculated by dividing the depth difference (mm) by the age difference (calibrated years).

https://doi.org/10.5194/egusphere-2026-3058
Preprint. Discussion started: 24 June 2026


### 2.3. Statistical treatment

For major and trace elements, mean concentration ± SD (mg $L^{-1}$) was calculated for the active and frozen layer at each site (Tz-1 (AL, n = 11), (FL, n = 18); Tz-2 (AL, n = 8), (FL, n = 20); Tz-3 (AL, n = 12), (FL, n = 16); and Tz-4 (AL, n = 8), (FL, n = 20)). Then, we determined which layer was more concentrated and calculated an enrichment ratio. Comparison of mean concentration for the active and the frozen layers at each site were explored through t-test if Shapiro-Wilk and Levene's test ($p > 0.05$) were both met; otherwise, we used Mann-Whitney ($p < 0.05$). Same statistical treatment was performed for (a) C contribution from organic acids (OA) (mg $L^{-1}$), SUVA254 and fluorescence index (FI) and (b) molar ratios C:N, N:P, and C:P (mol $L^{-1}$) (Mann-Whitney test, $p < 0.01$). For variables (a) and (b), between-site comparisons were processed using a H-criterion Kruskal-Wallis test ($p < 0.01$).
Principal component analysis (PCA) was used for the chemical elements set of sampled pore waters and permafrost ice, allowing to test distribution of DOC, TDN, DON, C from organic acids, major and trace elements (47 variables) preprocessed using log10(x+1) to reduce skewness and extreme values, as well as StandardScaler to equalize units (µg $L^{-1}$ and mg $L^{-1}$) for both active and frozen layers samples. The REE group is represented by Tm, since all elements except La, Y and Pr were highly correlated ($r > 0.6$). The centroid calculations were performed for all active layer and frozen layer samples, as well as for each site, and for the active and frozen layer within each site. Statistical treatment was performed using statistical libraries (scipy.stats and scikit-learn) along with matplotlib and seaborn plotting libraries in a Python environment.

### 2.4. Mass balance projections of C, N and P consumption and export

To assess the potential consequences of progressive active layer deepening, we quantified the *in situ* consumption and potential lateral export of DOC, TDN and TDP (g $m^{-2}$) from the pore ice reservoir under a thaw scenario (1 cm $yr^{-1}$ active layer deepening over the next 100 years after Åkerman and Johansson (2008)). The consumption–export model couples the constraints on dissolved organic matter (DOM) uptake— ICBM-style substrate kinetics and elemental stoichiometry (C:N:P) along with carbon use efficiency (CUE) (Byun et al., 2025). Further methodological detail is provided in the Supplementary Information (Table S3).

## 3 Results

### 3.1 Peatland formation and permafrost installation

Peatland formation in the Western Siberian Lowland (WSL) started approximately 9 ka ago and persisted throughout the Holocene (Vasil'chuk and Vasil'chuk, 2016). At the Tazovsky site, peatland establishment likely began during the Early Holocene, as indicated by the oldest dated sample at 8.4 cal kBP from 180 cm depth in Tz-4 (Table S1). In the WSL tundra, Early Holocene peat apparent accumulation rates were calculated at 1.4–1.6 mm $yr^{-1}$ (Fotiev, 2017), slightly higher than the value derived for the Tz-4 frozen layer (1.25 mm $yr^{-1}$ between 50–180 cm depth). During the Late Holocene, regional peat

https://doi.org/10.5194/egusphere-2026-3058
Preprint. Discussion started: 24 June 2026


accumulation rates declined to approximately 0.4 mm yr⁻¹, also reflected at Tz-3 (0.33 mm yr⁻¹) and Tz-1 (0.52 mm yr⁻¹). This shift is also recorded at Tz-4 transition from woody-grass peat to shrub–herbaceous peat at approximately 50 cm depth (7.4 cal kBP), followed by a sharp decrease in the upper layer of Tz-4 (0.1 mm yr⁻¹) (Figure S1).
Middle Holocene permafrost and local thermokarst turned a productive wetland into frost-heaved terrain (Tikhonravova et al., 2023), consequently increasing syngenetic formation of ice wedges between 5.3–3.4 cal kBP (Vasil'chuk et al., 2026) and polygon mounds raised the surface while adjacent lows stayed waterlogged (Raudina et al., 2017a). At Tz-2, erosion between 7.2 and 3.3 cal kBP stopped woody-grass peat, then Sphagnum took over—consistent with thermokarst-driven wetting and lower ice-wedge density in the lower polygonal setting. During the Subatlantic cooling phase (2.0–1.3 cal kBP), peatlands experienced renewed freezing, leading to frost mound formation and reactivation of the ice-wedge system (Kondratjeva et al., 1993). The most recent peat accumulation is observed at Tz-1 ($F^{14}C > 1$, Table S1), followed by Tz-3 and Tz-2 at 10 cm depth (0.3 and 0.2 cal kBP, respectively). In contrast, peat accumulation in the upper layers of Tz-4 ceased around 2.8 cal kBP.
This chronological framework indicates spatially asynchronous peat growth and freezing histories across the thaw gradient, with Tz-4 representing an older, long-stabilized frost mound, whereas Tz-1 and intermediate microsites reflect more recent or ongoing peat formation and hydrological connectivity. Together, the Holocene evolution of peat accumulation and permafrost installation in terms of freezing, frost heave, and thermokarst activity among microsites impacts contemporary freeze–thaw dynamics, preconditioning the DOM composition, nutrient storage and metal portioning between active and frozen layers.

### 3.2. Vertical profile of C, N and P concentration in active and frozen layer

Concentrations of DOC, TDN and TDP are illustrated in Fig. 2, along with C from organic acids concentrations, and N-$NH_4^+$ and P-$PO_4^{3-}$ to their respective pools. The vertical pattern of these major nutrient distribution exhibits systematically higher concentrations in the frozen layer **(**20–60 cm below the active layer boundary) compared to the active layer across all microsites**.** For TDN (Fig. 2b), low concentrations (< 15 mg L⁻¹) dominate the active layers, compared to frozen layers where the maximal concentrations are situated (Tz-4 at 130–160 cm, Tz-3 at 75–85 cm, Tz-2 and Tz-1 at 70–90 cm). P maxima are registered in the frozen layers for all microsites, although TDP concentration remains relatively stable throughout the soil column for Tz-1, and Tz-4 active layer is depleted except for most surficial point (Fig. 2c). Overall, DOC concentrations increase from the convex polygon (Tz-4) to the concave polygon and transitional fen (Tz-3 and Tz-2), before decreasing at fen (Tz-1), whereas TDN maxima shift progressively deeper. In contrast to DOC and TDN, phosphorus shows a stronger site-specific redistribution, with an increase in concentrations for the frozen horizons of the concave polygon and transitional fen (Tz-3 and Tz-2), whereas the convex polygon (Tz-4) and peat-mineral fen (Tz-1) display more uniform vertical profiles.

https://doi.org/10.5194/egusphere-2026-3058
Preprint. Discussion started: 24 June 2026


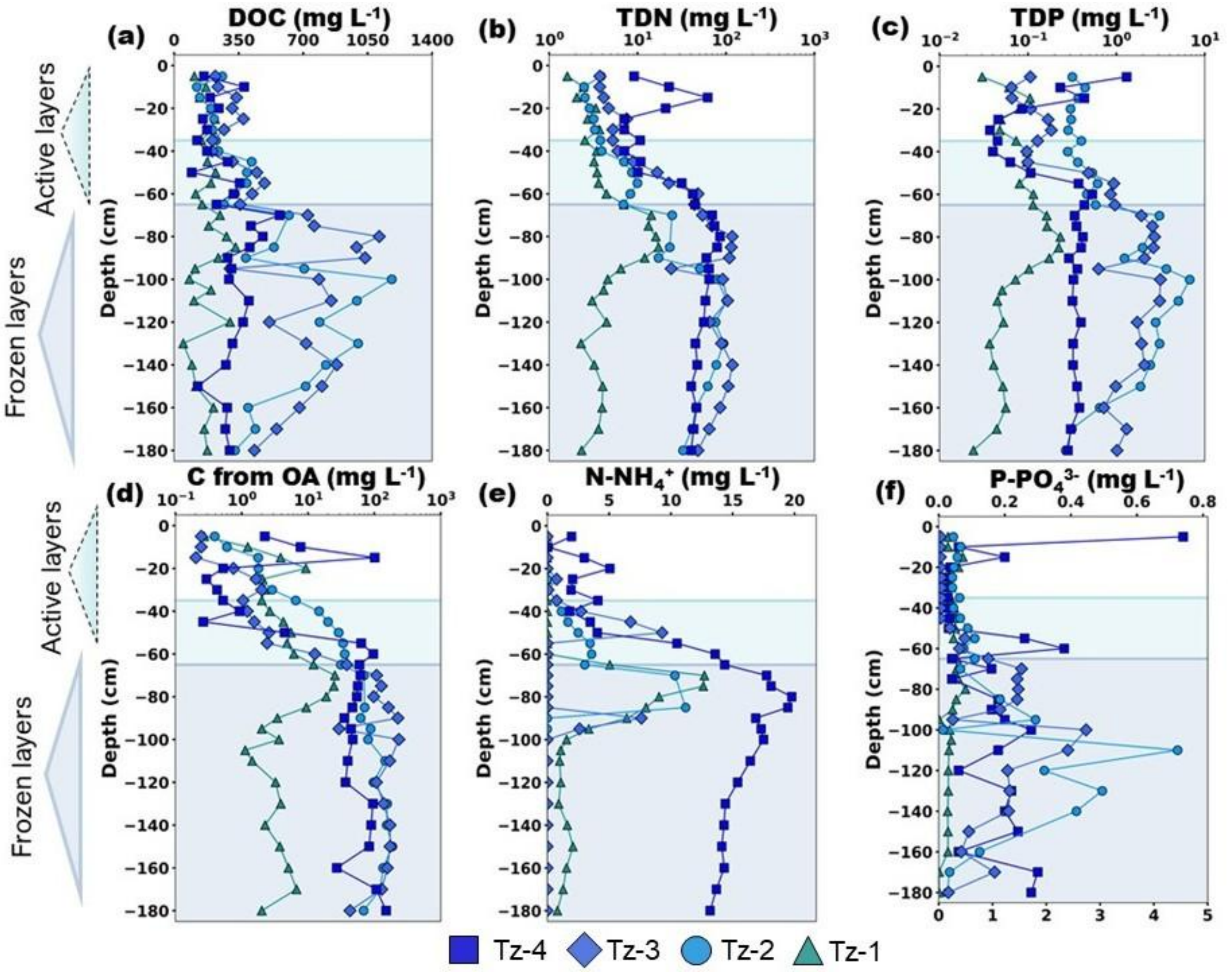


Figure 2. (Log)-profiles of dissolved (< 0.45 µm) (a) DOC, (b) TDN, (c) TDP, (d) C from Organic Acids (OA), (e) N-NH4+ and (f) P-PO43- (mg L-1) for porewater at the active layers and pore ice at the frozen layers. Upper concentration axis of (f) P-PO43- corresponds to site Tz-1 and Tz-4, whereas the lower axis shows values for Tz-2 and Tz-3. The lower limit of the active layer thickness is situated at 35 to 65 cm depth after sampling limits (Tz- = 155 ± 5 cm, Tz-2 = 40 ± 5 cm, Tz-3 = 60 ± 5 cm, and Tz-4 = 40 ± 5 cm). Permanent frozen layer is considered after 65 cm.

As for C derived from organic acids (Fig. 2d), all microsites show an increase in contribution of C from organic acids with depth, becoming more prominent in the frozen layer and with a more homogeneous distribution (Fig. S3). Maxima of N-$NH_4^+$ are also situated in the frozen layers for (Fig. 2e) except for Tz-3, although a secondary maximum can be found at 90 cm depth.

https://doi.org/10.5194/egusphere-2026-3058
Preprint. Discussion started: 24 June 2026


Although the TDN pool is predominantly composed of dissolved organic nitrogen (Fig. S2), N-$NH_4^+$ may represent (~30% of TDN on average through the soil column at Tz-4 (Fig. S3a) and more than 40 % at the bottom of the Tz-3 active layer (Fig. S3b). For Tz-2, N-$NH_4^+$ accounts for 20–48 % between 30 and 85 cm but decreases below 90 cm (Fig. S3c). In Tz-1 frozen layer, N-$NH_4^+$ represents > 50% of TDN between 65–95 cm and again at 140–150 cm, while the active layer shows depletion in N-$NH_4^+$ and a relative increase in N-$NO_3^-$ (Fig. S3d). The relative contribution of $NH_4^+$ to TDN increases in frozen horizons and becomes more dominant at deeper depths, contrary to DON dominated active layers, indicating progressive ammonium retention within the permafrost compartment toward more advanced thaw stages. In contrast, the contribution of $PO_4^{3-}$ to TDP shows no uniform monotonic trend along the thaw gradient (Fig. 2f, Fig. S4), but displays site-specific enrichment in the frozen layers of the concave polygon and transitional fen (Tz-3 and Tz-2), while remaining comparatively stable and lower in both the bog (Tz-4) and peat-mineral fen (Tz-1).

### 3.3. Molecular properties of DOC, distribution of organic acids and C:N:P ratios

Regarding the C pool, pore ice in peat-dominated microsites (convex polygon Tz-4 → concave polygon Tz-3 → peat transitional fen Tz-2) shows a significantly higher contribution from organic acids compared to the frozen mineral layer of Tz-1 (peat-mineral fen) (Fig. 3a). Across all microsites, pore ice is characterized by lower aromaticity than active layer porewaters (Fig. 3b), indicating selective preservation of less aromatic, more labile compounds in the frozen compartment. Along the thaw gradient (Tz-4 → Tz-1), frozen layers consistently shift toward a more microbially processed (FI > 1.4, Fig. 3c), while active layers retain a stronger plant-derived component, particularly in the convex and concave polygon systems (Table S2). Exceptionally, Tz-2 reflects a less significant difference between layers (Table S2).

https://doi.org/10.5194/egusphere-2026-3058
Preprint. Discussion started: 24 June 2026


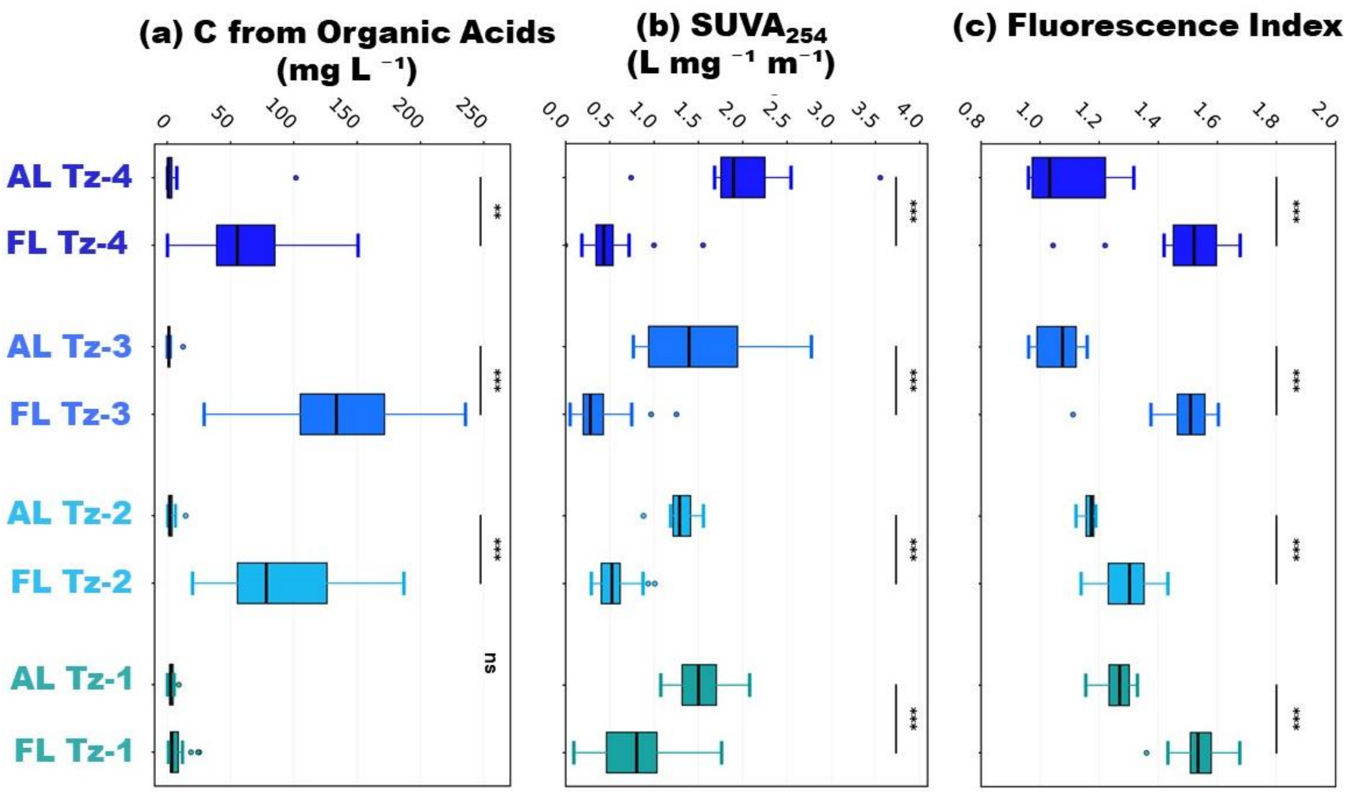


Figure 3. Whisker plots of porewater (AL) and pore ice (FL) dissolved phase (< 0.45 µm) for (a) C from Organic Acids (mg $L^{-1}$), (b) $SUVA_{254}$ (L $mg^{-1}$ $m^{-1}$) and (c) Fluorescence Index (FI). Concentrations for both layers were tested at each site using a non-parametric paired Mann-Whitney test ($p < 0.01$, **; $p < 0.001$, ***).

Carboxylic compounds represent up to 20 % of DOC pool in Tz-4 (median concentration, 55 ± 36 mg C $L^{-1}$), Tz-3 (138 ± 61 g C $L^{-1}$), and Tz-2 (78 ± 49 mg C $L^{-1}$) frozen layers, whereas carboxylic compounds median concentration in Tz-1 frozen layer pore ice (4 ± 7 mg C $L^{-1}$) falls in the same range of active layer porewaters (Tz-4 = 0.7 ± 35.0, Tz-3= 1.4 ± 3.4, Tz-2 = 1.8 ± 4. 8, Tz-1 = 2.7 ± 2.5 mg C $L^{-1}$). The relative abundance of each carboxylic compound within the total organic acid pool (Fig. S2) shows that frozen horizons across peat-dominated microsites (Tz-4, Tz-3, Tz-2) display a more homogeneous distribution dominated by low-molecular-weight acids (acetate, formate, glycolate), also reflected in higher concentrations of these compounds relatively to the active layers (Fig. S5). On the contrary, the peat-mineral fen (Tz-1) retains greater compositional variability. Overall, the thaw gradient is characterized by a progressive simplification of the organic acid spectrum from the active layer to the frozen layer.

https://doi.org/10.5194/egusphere-2026-3058
Preprint. Discussion started: 24 June 2026


Lower median C:N ratios occur significantly in frozen than in active layers at every site (Tz-4 = 7, $p < 0.01$; Tz-3 = 10, $p < 0.01$; Tz-2 = 22, $p < 0.001$; Tz-1 = 28, $p < 0.01$; Fig. 4a). At the bog (Tz-4) and through (Tz-3) systems, the N:P ratio (Fig. 4b) is not significantly different between the active and frozen layers (Table S3), and the significant active–frozen contrasts appear only at Tz-1 ($p < 0.001$; 88 vs 164) and Tz-2 ($p < 0.01$; 22 vs 38). C:P ratios are lower in frozen horizons (Tz-4 = 2439, Tz-3 = 1016, Tz-2 = 856, Tz-1 = 3901; Fig. 4c) compared to active layers but statistically significant only at Tz-3 ($p < 0.001$). Along the thaw gradient (convex polygon Tz-4 → concave polygon Tz-3 → transitional fen Tz-2 → peat–mineral fen Tz-1), frozen layers show progressively higher C:N and highly variable C:P, while N:P rises most at intermediate to advanced thaw (Tz-2, Tz-1). Collectively, the permafrost compartment is marked by lower C:N and C:P but relatively higher N:P than active layers, indicating differential retention and redistribution of C, N, and P across the active-layer–permafrost interface.

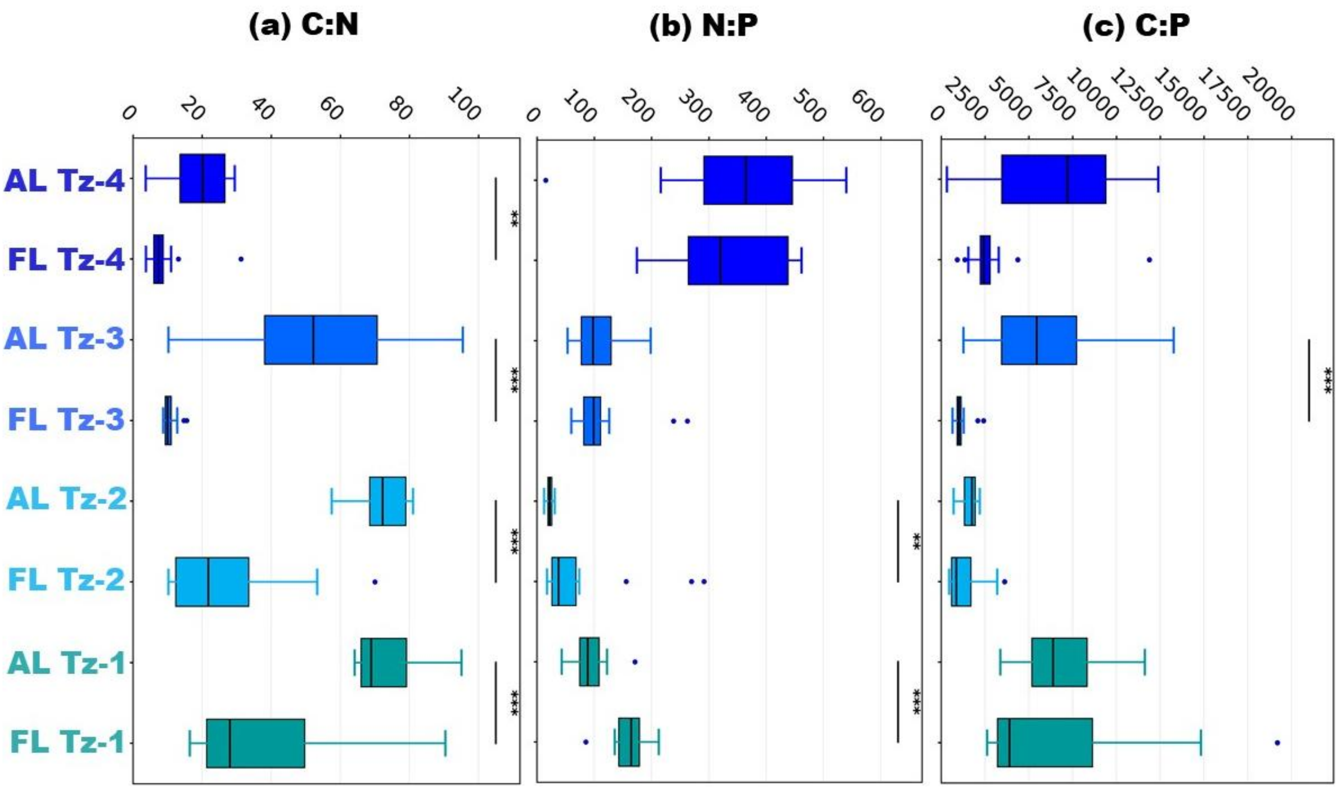


Figure 4. Whisker plots of porewater (AL) and pore ice (FL) dissolved phase (< 0.45 µm) for (a) C:N, (b) N:P and (c) C:P (mol $L^{-1}$: mol $L^{-1}$). Concentrations for both layers were tested at each site using a non-parametric paired Mann-Whitney test ($p < 0.01$, **; $p < 0.001$, ***).

https://doi.org/10.5194/egusphere-2026-3058
Preprint. Discussion started: 24 June 2026


### 3.4. Mass balance projections of C, N and P consumption and export under active layer deepening

280 Model outputs indicate that CNP stoichiometry enhances the C and N export, as TDP is largely consumed *in situ* before potential export (Table 1). Phosphorus limitation dominates most horizons (f_P < 1), whereas N is generally non-limiting (f_N > 1; Table S4). N consumption represents only 1.06–3.97 % of total N pools, indicating substantial N carryover between horizons. Projected C consumption under 100 cm thaw remains limited (1.87 % at Tz-1, 12.53 % at Tz-2, 10.17 % at Tz-3, and 3.93 % at Tz-4). In contrast to TDP, most DOC and TDN are projected to be exported via suprapermafrost flow (Table 1),
285 with export estimates falling within the range reported for Arctic peatlands (Olefeldt and Roulet, 2012), and consistent with observations from Arctic hillslopes where N is rapidly flushed downslope (Harms and Ludwig, 2016). Overall, model results indicate that progressive active layer deepening preferentially mobilizes DOC and TDN, while TDP is largely retained through *in situ* microbial consumption, suggesting differential nutrient export responses under gradual thaw.

290 Table 1. Consumption (respired and locked in biomass) and potential export for DOC, TDN and TDP for a 100 cm active layer deepening for each site.

| | DOC (g C $m^{-2}$ $yr^{-1}$) | | TDN (g N $m^{-2}$ $yr^{-1}$) | | TDP (g P $m^{-2}$ $yr^{-1}$) | |
|---|---|---|---|---|---|---|
| **Site** | **Consumption** | **Potential export** | **Consumption** | **Potential export** | **Consumption** | **Potential export** |
| Tz4 | 0.142 | 3.465 | 0.005 | 0.554 | 0.004 | 0.000 |
| Tz3 | 0.796 | 7.032 | 0.030 | 0.890 | 0.020 | 0.000 |
| Tz2 | 0.842 | 5.874 | 0.019 | 0.465 | 0.026 | 0.000 |
| Tz1 | 0.020 | 1.040 | 0.000 | 0.041 | 0.001 | 0.000 |

### 3.5. Major and trace inorganic solutes

The depth patterns of element concentration in peat porewater and ice are represented for selected elements in Figure 5.
295 Potassium concentrations (Fig. 5a) remain relatively stable within the frozen layers across all microsites, whereas active layers show a general decrease with depth, interrupted by shallow peaks (15 cm for Tz-4, 5 cm for Tz-2 and Tz-3).

Calcium exhibits a systematic increase from the active to the frozen layers at all sites (Fig. 5b), with the strongest vertical gradient observed in the peat-dominated microsites (Tz-4, Tz-3 and Tz-2), with a less pronounced increase at Tz-2 (peat transitional fen).

300 Titanium, Vanadium and Iron (Fig. 5c–e) display site-specific patterns. For Tz-4 (bog), Ti, V and Fe show higher concentrations in the active layer followed by an abrupt decrease at the active layer–frozen layer boundary (45–55 cm). In contrast, Fe concentrations at Tz-3, Tz-2 and Tz-1 increase with depth, reaching maxima within the frozen layer (85 cm for

https://doi.org/10.5194/egusphere-2026-3058
Preprint. Discussion started: 24 June 2026


Tz-3 and Tz-1; 100 cm for Tz-2), whereas Tz-4 exhibits a decrease across the boundary and relatively stable concentrations throughout the frozen layer (Fig. 5e). Arsenic concentrations increase with depth at all sites (Fig. 5f), with a sharp transition at the base of the active layer.

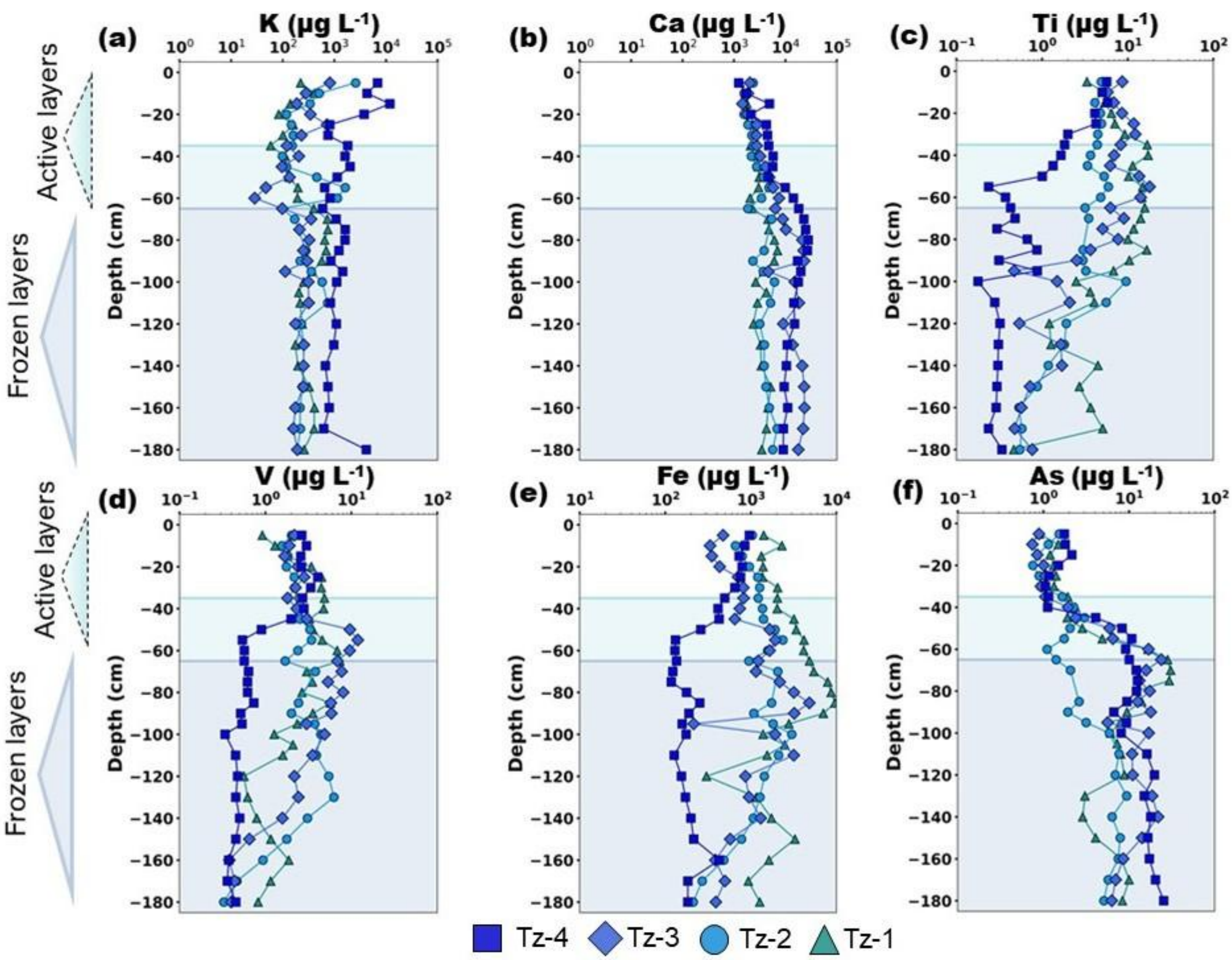


Figure 5. Log profiles of dissolved (< 0.45 µm) (a) K, (b) Ca, (c) Ti, (d) V, (e) Fe and (f) As (µg L-1) for porewater at the active layers and pore ice at the frozen layers. The lower limit of the active layer thickness is situated at 35 to 65 cm depth after sampling limits (Tz-= 155 ± 5 cm, Tz-2 = 40 ± 5 cm, Tz-3 = 60 ± 5 cm, and Tz-4 = 40 ± 5 cm). Permanent frozen layer is considered after 65 cm.

Overall, labile divalent cations (Ca, Mg, Mn, Sr) and several trace elements (Fig. S7, Table S5) display consistent enrichment in frozen horizons relative to active layers, indicating preferential accumulation within the permafrost compartment. This trend

https://doi.org/10.5194/egusphere-2026-3058
Preprint. Discussion started: 24 June 2026


is especially pronounced in peat-dominated microsites (Tz-4 → Tz-3 → Tz-2), while the peat-mineral fen (Tz-1) exhibits weaker or absent enrichment for certain components (DOC, TDP, Ba) (Table S5). A distinctive enrichment pattern in the bog (Tz-4) active layer contrasts with the general trend of frozen-layer accumulation along the thaw gradient, as only Tz-4 shows significant enrichment of active layer porewaters in rare earth elements (La, Ce, Pr, Nd, Sm, Eu, Gd, Tb, Dy, Ho, Er, Tm, Yb, Lu), lithogenic trace elements (Y, Zr, Hf, W), and metalloids including Ge, Ga and Se, as well as micro-nutrients Fe, Co, Ni and Mo (Table S5). Solute partitioning shows a shift from active-layer enrichment of lithogenic and transition elements in the bog (Tz-4) toward increasingly pronounced frozen-layer enrichment of major cations and selected trace elements in the concave polygon and transitional fen (Tz-3 and Tz-2). The peat-mineral fen (Tz-1) displays a more subdued contrast between compartments, suggesting progressive reorganization of inorganic solute storage across thaw stages.

### 3.6. PCA Treatment of major and trace solutes

To further explore relationships among major and trace elements, a PCA was performed separately for active layer porewaters and frozen layer pore ice at the four sites (Fig. 6). For all samples combined, PC1 and PC2 explain 54.7 % of the cumulative variance, while inclusion of PC3 increases the explained variance to 67.0 %. PC1 is primarily driven by lithogenic hydrolysates (Zr, Ga, Hf, Ge, Nb, Cr, Y and La), whereas PC2 is controlled by TDN, Sr, Ca, C from OA, DOC, TDP, $SO_4^{2-}$ and Ba. PC3 is associated mainly with most labile Na, Li, and Mg. A clear compositional structuring between active and frozen compartments across sites arises from corresponding centroid calculations (Euclidean distance = 4.56, $p = 0.0005$), and active- frozen layer separation is predominantly structured along PC2 (Glass's $\Delta = -1.44$, $p < 0.0001$), followed by PC3 (Glass's $\Delta = -0.75$, $p = 0.0009$) and PC1 (Glass's $\Delta = +0.37$, $p = 0.02$), indicating that organic solutes and exchangeable cations exert stronger control on compartment differentiation than lithogenic elements. Active layer samples show lower dispersion around their centroid (3.27 ± 2.69) compared to frozen samples (5.26 ± 1.98) ($p < 0.001$), suggesting greater compositional homogenization within active layer porewaters contrary to frozen samples, reflecting greater vertical and site-specific variability in pore ice chemistry (Fig. S8, Fig. 6). For example, most Tz-4 frozen samples show minimal variation along PC1, indicating compositional stability within this microsite.

The dispersion of frozen samples is partly influenced by pronounced depth-specific peaks, which appear as outliers in ordination space. Depth-resolved PCA projections (Fig. S9) illustrate these patterns in detail. The PC2 axis highlights the preferential association of DOC, TDN and TDP with exchangeable cations (Ca, Mn, Ba, Sr), indicating coherent grouping of DOM-related solutes in pore ice (Table S5). This axis therefore captures the dominant vertical partitioning pattern between nutrient-enriched frozen horizons and comparatively lithogenic-dominated active porewaters. Conversely, PC1 reflects enrichment of lithogenic, low mobility hydrolysates (Zr, Ga, Hf, Ge, Nb, Cr, Y and REEs) in active layer porewaters. Overall, PCA confirms that vertical compartmentalization (active vs frozen layer) represents the primary structuring factor of dissolved solute composition, exceeding spatial variability among microsites. Frozen layers are characterized by greater compositional dispersion and site clustering, whereas active layers show stronger homogenization. The ordination thus reinforces the

https://doi.org/10.5194/egusphere-2026-3058
Preprint. Discussion started: 24 June 2026


observed partitioning of DOM and exchangeable cations into pore ice, while lithogenic and transition elements preferentially remain associated with active layer porewaters (Fig. 6; Fig. S9; Table S5).

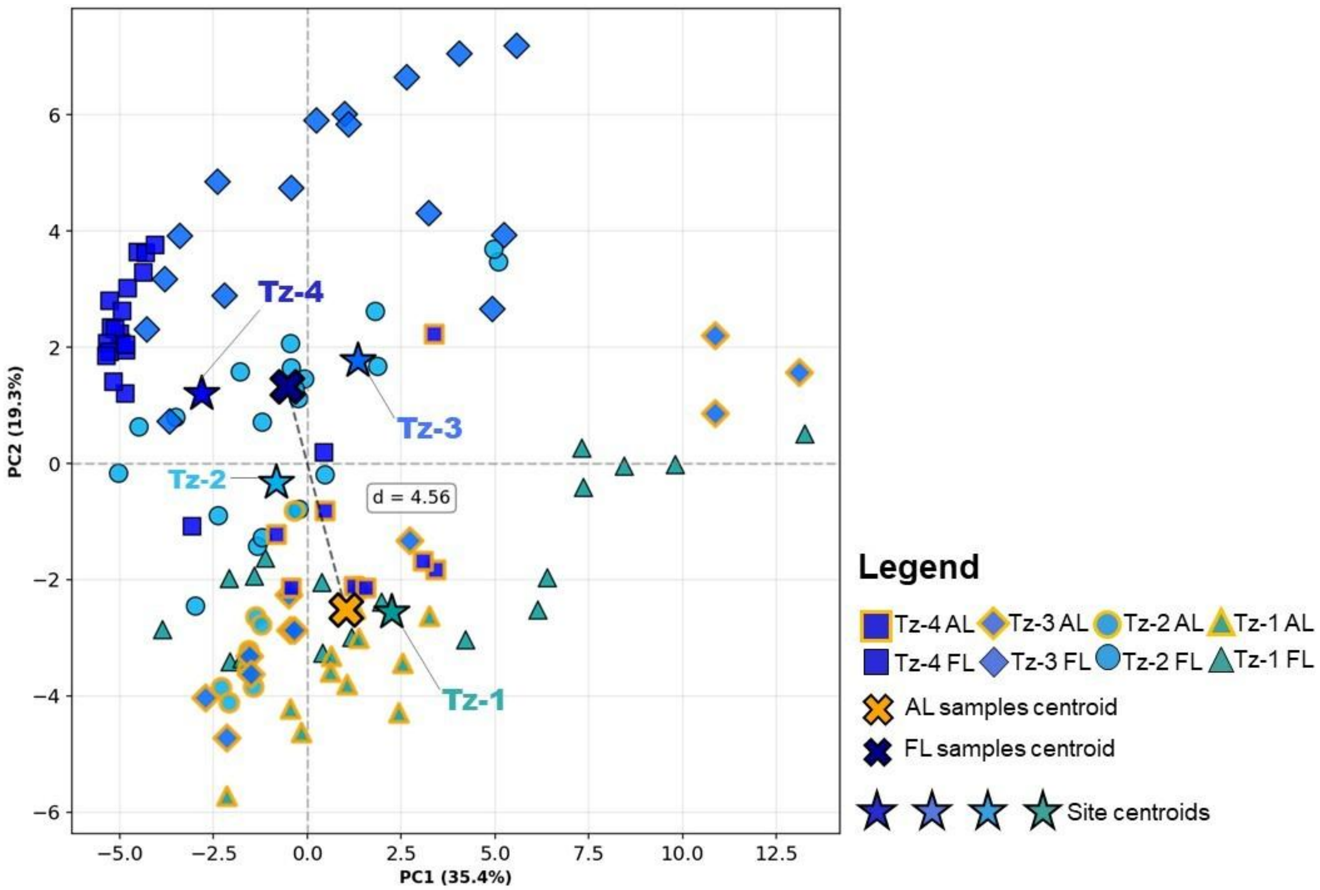


Figure 6. Two-dimensional PCA projection (PC1 vs PC2) of active layer porewater (n = 39) and frozen layer pore ice (n = 74) samples. Centroid coordinates for PC1–PC3 are (+0.97, −2.40, −1.08) for active samples and (−0.51, +1.26, +0.57) for frozen samples, respectively. Site-specific centroids (Tz-4, Tz-3, Tz-2 and Tz-1) are also shown.

## 4 Discussion

### 4.1. Freeze–thaw controls on C–N–P partitioning across the active layer–permafrost interface

Taken together, the vertical profiles of organic and inorganic solutes reveal coherent co-variations of C, N, P and major–trace elements along the thaw sequence (convex polygon Tz-4 → concave polygon Tz-3 → transitional fen Tz-2 → peat-mineral fen Tz-1). The contrasting chemical signatures observed between active layer porewaters and frozen pore ice indicate that

https://doi.org/10.5194/egusphere-2026-3058
Preprint. Discussion started: 24 June 2026


freeze–thaw cycles (FTC) act as a major organizing mechanism for carbon and nutrient partitioning in polygonal peatlands, specifically for nitrogen transformations, and phosphorus redistribution across the thaw gradient.

Peat accumulation rates and seasonal freezing may explain the absence of certain compound peaks, as polygonal mounds can lengthen solute residence time (less water loss and reduced hydraulic conductivity) and thus concentrate pore fluids (Raudina et al., 2017), whereas troughs exhibit higher annual temperatures resulting in a deeper seasonal thaw (Armstrong, 2012; Raudina et al., 2025). Successive FTC may promote downward transfer of solutes from the active layer to underlying frozen horizons along thermal gradients. Fragmentation of large DOM molecules and removal of aromatic carbon (Pokrovsky et al., 2018a), along with an enrichment in aliphatic low-molecular-weight organic matter (Payandi-Rolland et al., 2021) enhanced by FTC, add to the contribution of low-molecular-weight molecules (e.g., root exudates) produced in the surface and upper active layers which are preferentially mobilized along with top-down freezing (Lim et al., 2022), consistent with the observed dominance of aliphatic compounds and higher organic acid concentrations in frozen layers (C).

Rapid peat accumulation and persistent saturation generate anoxic conditions; in anoxic fen microcosms, fermentation of cellulose, glucose and xylose produces butyrate and propionate (Schmidt et al., 2016). Lactate and acetate, primary pyruvate formation products, occur at very low concentrations in shallow horizons of northern peatlands (Wang et al., 2024), and significantly depleted in active layers relative to pore ice ($p < 0.001$, Fig. S5), indicating preferential microbial consumption in the active layer compartment, consistent with observations in the sporadic permafrost peatlands (Kuzmina et al., 2023).

Nitrogen cycling mirrors many of these carbon-driven processes. The active layer experiences aggregate disruption under FTC, exposing previously protected soil organic matter (SOM) to microbial mineralization (Feng et al., 2007), enriching DON subsequently to be mineralized to $NH_4^+$ through ammonification. Under oxic microsites, $NH_4^+$ may undergo nitrification ($NH_4^+ \rightarrow NO_2^- \rightarrow NO_3^-$), but rapid return to anoxic conditions favors dissimilatory nitrate reduction to ammonium (DNRA), limiting nitrate accumulation by prevailing anoxia (Logan et al., 2025). This sequence explains the generally low proportion of $NO_3^-$ relative to $NH_4^+$ across sites (Fig. S3). At Tz-1, $NH_4^+$ accounts for up to 90 % of TDN in the frozen layer (Fig. S3d), suggesting strong mineralization and possible downslope transport of inorganic N from upper microsites (Tz-3 and Tz-2) toward lower-lying areas during drainage (Pedersen et al., 2022). The presence of $NH_4^+$ at the base of active layers in Tz-3 (25–50 cm) and Tz-2 (35–85 cm) likely reflects contemporary microbial activity at the thaw boundary. In frozen layers, contrasting patterns emerge: Tz-3 is dominated by DON, whereas Tz-4 exhibits relatively stable $NH_4^+$ concentrations (~15 mg $L^{-1}$, ~30 % of TDN; Fig. 2e), possibly indicating rapid freezing during permafrost installation that limited DNRA progression. Overall, N partitioning suggests that freeze–thaw dynamics favor ammonium accumulation in frozen compartments, while active layers remain zones of rapid organic N turnover and transformation.

Phosphorus dynamics are similarly influenced by FTC but are additionally constrained by enzymatic controls. Particle fragmentation induced by freezing can increase organic P mobilization, as demonstrated for river ice incorporating sediment-derived P (Zhang et al., 2022). In peatlands, FTC may therefore liberate P from soil organic matter. However, enzymatic activity—particularly phosphatases—is required to convert organic P into bioavailable phosphate (Park et al., 2022). In Arctic systems, P turnover is strongly governed by microbial dynamics (Chapin et al., 1978), and microbial biomass represents a

https://doi.org/10.5194/egusphere-2026-3058
Preprint. Discussion started: 24 June 2026


major reservoir of potentially available P (Giblin et al., 1991). TDP enrichment in pore ice from Tz-4 to Tz-2 (Table S3) suggests preferential incorporation or preservation of dissolved P in frozen horizons, although peak concentrations are not systematically associated with increased $PO_4^{3-}$ contribution (Fig. S4). This indicates that freeze–thaw processes may redistribute total dissolved P without uniformly enhancing inorganic phosphate dominance, implying coupled controls of physical redistribution and biological mineralization.

In summary, freeze–thaw cycles reorganize C–N–P pools across the active layer–permafrost interface by (i) selectively retaining low-molecular-weight, microbially derived DOM in frozen horizons; (ii) promoting ammonium accumulation while limiting nitrate persistence; and (iii) redistributing dissolved phosphorus through combined physical fragmentation and enzymatic mediation. The active layer thus functions as a zone of rapid biological turnover, while the frozen layer acts as a reservoir integrating both cryogenic fractionation and legacy microbial processing–explaining C–N–P stoichiometric contrasts along the thaw gradient and underscores the central role of freeze–thaw dynamics in shaping nutrient export potential from permafrost peatlands.

### 4.2. Bioavailability and redox sensitivity of C–N–P pools in pore ice

Building on the partitioning patterns discussed above, we now assess the potential bioavailability of pore ice solutes and their implications for biogeochemical reactivity regarding microbial mineralization, nutrient cycling and greenhouse gas production upon-thawing. Frozen horizons store a chemically labile and readily metabolizable DOM pool **(**FI > 1.4, higher concentrations of C from organic acids, and $SUVA_{254}$ < 2). Seasonal production and downward leaching of $NH_4^+$ toward the thaw front suggests rapid reactivation of N cycling upon thawing synchronously with carbon mineralization processes (Fouché et al., 2020). Amplification of FTC stimulated microbial N metabolism along with recalcitrant soil organic carbon driven by $NH_4^+$ pool consumption (Yan et al., 2025).

Given the dominance of aliphatic DOM in pore ice, strong aromatic binding appears unlikely (Hamdan et al., 2012), indicating that a fraction of pore ice P may be readily available upon thaw. The non-phosphate TDP fraction may include organic P compounds derived from microbial cell lysis during FTC, as laboratory studies show that release of labile organic matter from microbial necromass enhance microbial mineralization (up to 65 % of the $CO_2$ efflux) following thaw (Herrmann and Witter, 2002). Labile DOM additions increase $CO_2$ production by 30–40 % in the lower active layer and 50–70 % in the permafrost (Walz et al., 2017), demonstrating sizable potential of thaw-released substrates even at low temperatures (Garcia-Pausas and Paterson, 2011), thereby reinforcing positive priming effects (Estop-Aragonés et al., 2022). Thus, pore ice may act not merely as a passive reservoir but as a biochemical trigger upon thaw, accelerating both carbon mineralization and coupled nutrient transformations in overlying active layers. In addition, mineralization is constrained by oxidation of organic matter controlled by thermodynamic hierarchies, with microorganisms utilizing inorganic terminal electron acceptors (TEAs) such as $NO_3^-$, Mn(III/IV), Fe(III) and $SO_4^{2-}$ prior to methanogenesis (Bridgham et al., 2013). The absence of nitrates suggests an oxygen depletion associated with contemporary FTC at the limit of the active-frozen layer (e.g., 60–70 cm in Tz-4; 55–65 cm in Tz-

https://doi.org/10.5194/egusphere-2026-3058
Preprint. Discussion started: 24 June 2026


3), also found in deeper anoxic layers (e.g., 100–140 cm in Tz-2) that represent paleo freeze–thaw fronts. Reductive pathways are favorized under prolonged water residence times, preventing oxygen replenishment after microbial consumption (Rooney et al., 2024). As cumulative freeze-thaw history is integrated in pore ice chemistry, it may also influence redox conditions upon thawing. Mn enrichment in pore ice (Table S5) suggests potential Mn reduction during anoxic phases. Subsequent reductive dissolution of Fe oxides may release previously bound phosphates (Barczok et al., 2024), although persistent saturation could deplete Fe-bound P pools, only moderated by binding competition to Al(III), less sensitive to redox fluctuations (Reddy and DeLaune, 2008). Sulfate depletion in active layer porewaters at Tz-3 and Tz-2 relative to pore ice peaks (Fig. S7) suggests sulfate reduction under saturated conditions (Lipson et al., 2013). After depletion of alternative TEAs, acetoclastic and hydrogenotrophic methanogenesis may dominate in acidic, saturated environments (Kotsyurbenko et al., 2004), although acetate may also be oxidized to $CO_2$ *via* aerobic respiration or Fe reduction (Duddleston et al., 2002). Furthermore, Fe–organic carbon associations may reduce net $CH_4$ emissions in anoxic permafrost peatlands (Voggenreiter et al., 2025), particularly where Fe(III)-reducers and anaerobic methanotrophs are active. Subsequent redox transitions determine whether released substrates stimulate $CO_2$ production, methane generation, or nutrient mobilization upon thawing. Thus, pore ice represents both a cryogenic archive of past biogeochemical processing and a reactive pool capable of amplifying future carbon and nutrient fluxes under continued permafrost warming.

#### 4.3. Cryogenic partitioning of major and trace elements across the thaw gradient

As the freezing front migrates downward, two principal groups of solutes are expected: those incorporated into the forming ice matrix and those excluded into the residual liquid phase through cryoconcentration, provided they do not undergo coagulation or precipitation (Ivanova et al., 2023). The alkaline earth metals (Mg, Ca, Sr) and divalent transition metals (Mn, Zn) exhibited significant enrichment in the aliphatic-dominated pore ice of frozen layers (Table S5), which suggests a preferential incorporation of hydrated and weakly complexed cations within the ice matrix or their association with low-molecular-weight (LMW) organic ligands that remain stable during freezing**.** Similar behavior has previously been reported for LMW organic colloids in surface waters (Pokrovsky et al., 2018b), and trace metals such as Cu and Ni, known to form strong complexes with LMW organic ligands (Wu and Tanoue, 2001; Xue et al., 1996), were also reported to be preferentially enriched in the ice relative to active layer porewaters in mineral soil cores (Lim et al., 2022).
Given the relatively rapid permafrost installation at Tz-4 and the apparent long-term stability of its frozen horizon, lithogenic elements such as REE appear to remain largely confined to organic and organo-mineral (Fe, Al) colloidal fractions(Lim et al., 2025b) within the active layer (Normalized Enrichment Factor, NEF $\approx -0.7$, $p < 0.001$) (Table S5) suggesting that cryogenic processes do not substantially redistribute strongly hydrolyzed or mineral-bound trace elements along the soil column. In the present study, a clear geochemical partitioning emerges for three dominant behavioral clusters: (*i*) DOM-related solutes and exchangeable cations that co-vary and accumulate in pore ice; (*ii*) lithogenic and high-field-strength elements that remain preferentially in active porewaters; and (*iii*) alkali and alkaline earth elements (Na, Li, Mg) showing depth-dependent variability, possibly reflecting ionic strength gradients and diffusive redistribution during freezing.

https://doi.org/10.5194/egusphere-2026-3058
Preprint. Discussion started: 24 June 2026


When interpreted in light of the PCA results, this element partitioning follows a coherent thaw-chronosequence pattern (convex polygon Tz-4 → concave polygon Tz-3 → transitional fen Tz-2 → peat-mineral fen Tz-1). In the convex polygon (Tz-4), the strongest centroid separation between active and frozen compartments reflects pronounced compartmentalization, with lithogenic and high-field-strength elements (Zr, Ga, Hf, Ge, Nb, Cr, Y, REEs) clustering along PC1 and remaining enriched in active porewaters. Moving toward the concave polygon (Tz-3) and transitional fen (Tz-2), frozen layers become increasingly structured along PC2, grouping DOC, TDN, TDP and labile cations (Ca, Mn, Sr, Ba), indicating preferential incorporation of DOM-associated and exchangeable solutes into pore ice at intermediate thaw stages. In the peat-mineral fen (Tz-1), the compartmental contrast weakens for several elements, suggesting enhanced hydrological connectivity and partial redistribution that attenuates the frozen-layer enrichment signal. Along the thaw sequence, intermediate stages (Tz-3 and Tz-2) maximize the coupling between DOM and exchangeable cations in frozen horizons, whereas advanced thaw (Tz-1) promotes partial flushing or redistribution of these pools. Freeze–thaw cycles not only concentrate nutrient-associated and exchangeable elements within pore ice but also maintain lithogenic and mineral-bound elements within the active layer. This dual behavior reinforces the interpretation that pore ice functions as a selectively enriched reservoir of labile C–N–P–cation complexes and, consequently, thaw progression reorganizes both the magnitude and the nature of metal–organic coupling across the active layer–permafrost interface.

### 4.4. Consequences of active layer deepening for *in situ* processing and riverine export

Siberian tundra permafrost is projected to warm at rates up to 0.056 °C $yr^{-1}$ (Vasiliev et al., 2020), resulting in active layer deepening of approximately 0.7–1.3 cm $yr^{-1}$ in continuous permafrost regions (Åkerman and Johansson, 2008). Abrupt thaw can trigger rapid carbon release, whereas gradual deepening favors lateral release of smaller quantities, enhancing *in situ* mineralization prior to export (Hamm et al., 2025). In Tazovsky, suprapermafrost waters exhibit highest concentrations of DOC, K, P, Fe, Cr and Cd during transitional stages, with concentrations declining in small water bodies and thermokarst lakes (Raudina et al., 2017; Lim et al., 2025; Loiko et al., 2026). Production of $CO_2$ and $CH_4$ in small water bodies is likely linked to nutrient consumption during transitional stages, implying that a fraction of released solutes may be mineralized before reaching downstream systems. Solute export from permafrost peatland watersheds depends primarily on the amount of water passing through unfrozen peat layers above the permafrost boundary before discharge to the riverine network (Hayashi et al., 2004; Wright et al., 2009; Raudina et al., 2018; Loiko et al., 2019). Modeled DOC export in this study at the concave polygon and peat transitional fen (7.03–5.87 g $m^{-2}$ $yr^{-1}$) falls in the same range as annual DOC fluxes in Arctic watersheds (Gandois et al., 2021). In the WSL permafrost catchments, the biennial DOC flux is estimated at 4.48–8.20 g $m^{-2}$ $yr^{-1}$ (Pokrovsky et al., 2020), so current riverine export may increase by degrading permafrost peatland contribution (7.83–1.06 g $m^{-2}$ $yr^{-1}$).
Water residence time increases from transitional fen to polygons (Tz-2 < Tz-3 < Tz-4), promoting initial flushing followed by depletion of newly available solutes (Loiko et al., 2019). Increased groundwater contribution may enhance transport of labile

https://doi.org/10.5194/egusphere-2026-3058
Preprint. Discussion started: 24 June 2026


solutes in the hydrological continuums in the WSL territory (Krickov et al., 2026), whereas DOC and DOC-trace metals complexes adsorption on mineral horizons can attenuate downward migration of C and low-mobile colloidal trace elements (Lim et al., 2022). Laboratory experiments suggest frozen-derived leachates may initially resemble pore ice composition (Ivanova et al., 2023b), yet gradual thaw is expected to modify colloidal vs dissolved fractions (Lim et al., 2021, 2025a). Consequently, an elevated loading on HREE may serve as a thaw indicator (Baxter et al., 2025), although REE distributions reflect local soil properties and drainage (Table S5).

Gradual active layer deepening is likely to enhance DOC and TDN export while maintaining partial *in situ* retention of phosphorus, whereas abrupt thaw may shift system behavior toward enhanced mineralization efficiency and altered microbial stoichiometry (Qin et al., 2025). Microbial degradation of thawed substrates and subsequent transformation into $CO_2$ or $CH_4$ is influenced by oxygen availability (Walz et al., 2017), pH (Monteux et al., 2018),and temperature (Kirkwood et al., 2021), and significantly on microbial adaptation to post-thaw conditions (Li et al., 2024), along with metabolic potential linked to permafrost age (Ji et al., 2020). As formerly observed in discontinuous permafrost peatlands in Western Siberia, spatially variability of C dynamics is linked to microhabitat -specific responses upon thawing (Halaś et al., 2025). Therefore, the role of micro-landscape in pore ice formation and composition, along with spatial position and hydrological residence time in the thaw sequence framework (Tz-4 → Tz-3 → Tz-2 → Tz-1), provides an insight into future consumption and export trajectories. The convex polygon (Tz-4) represents a long-stabilized system with strong vertical compartmentalization and longer residence times, favoring *in situ* processing. The concave polygon and transitional fen (Tz-3 and Tz-2) illustrate intermediate thaw stages where pore ice reservoirs are maximally mobilized and DOM–cation coupling is strongest, potentially enhancing export pulses. The peat-mineral fen (Tz-1), characterized by greater hydrological connectivity, reflects a more advanced thaw state in which redistribution and flushing reduce compartmental contrasts and increase the likelihood of lateral solute transfer. Thus, the thaw chronosequence suggests a transient amplification of nutrient-rich export at intermediate stages, followed by stabilization or redistribution under advanced thaw conditions.

## 5 Conclusions

This study demonstrates that freeze–thaw dynamics fundamentally structure the partitioning of carbon, nutrients and metals between active layer porewaters and frozen pore ice in continuous permafrost peatlands. Across the Tazovsky thaw sequence, pore ice consistently accumulated microbially processed, low-aromatic and low-molecular-weight organic-acid-rich DOM, whereas active layer porewaters retained a stronger lithogenic and mineral-associated signature. This cryogenic partitioning reflects selective incorporation of LMW DOM and labile cations into the frozen matrix, while high-field-strength and mineral-derived elements remain preferentially associated with the seasonally thawed compartment.

Stoichiometric patterns reinforce this vertical differentiation. Frozen horizons exhibit systematically lower C:N and C:P ratios relative to active layers, indicating preferential retention of nitrogen and phosphorus relative to carbon within the permafrost compartment. In contrast, N:P ratios vary more strongly along the thaw chronosequence, suggesting that landscape-scale thaw progression modulates nutrient balance beyond vertical freeze-induced fractionation. Multivariate analysis (PCA) confirms that vertical compartmentalization exerts a stronger control on solute composition than spatial variability among microsites, while intermediate thaw stages maximize the coupling between DOM and exchangeable cations in pore ice.

Model projections of progressive active layer deepening indicate differential fates for C, N and P. Phosphorus is largely consumed *in situ* under stoichiometric limitation, whereas DOC and TDN are more likely to be exported laterally via suprapermafrost flow. Thus, gradual thaw preferentially enhances carbon and nitrogen mobility, while maintaining partial phosphorus retention within the peat column. The balance between *in situ* mineralization and lateral export is further regulated by water residence time and hydrological connectivity along the thaw gradient.

Interpreted through a space-for-time framework (convex polygon → concave polygon → peat transitional fen → peat-mineral fen), the thaw sequence suggests a transient amplification of nutrient-rich pore ice mobilization at intermediate stages, followed by increasing redistribution and flushing under advanced thaw. Consequently, permafrost peatlands may experience a phase of enhanced carbon and nutrient reorganization prior to large-scale permafrost loss. Overall, pore ice acts both as a cryogenic archive of past biogeochemical processing and as a chemically reactive reservoir poised for rapid transformation under continued warming. By linking cryogenic fractionation, stoichiometric constraints, multivariate solute structure and export projections, this study provides a mechanistic basis for anticipating how progressive active layer deepening may reshape high-latitude carbon and nutrient fluxes, with implications for Arctic rivers chemistry and climate feedbacks.

## Code and data availability

All data supporting this study are publicly available via Zenodo at repository 10.5281/zenodo.20059630.

## Supplement link

The link to the supplement will be included by Copernicus, if applicable.

## Author contributions

LPS wrote the manuscript draft and participated in investigation, data curation and formal analysis. SVL contributed to funding acquisition, investigation and methodology. AL participated in data curation, investigation and methodology. LG participated in investigation and validation. CH collaborated on data curation and validation. JLR and OSP validated the research outputs, reviewed and edited the manuscript, and contributed with funding acquisition.

https://doi.org/10.5194/egusphere-2026-3058
Preprint. Discussion started: 24 June 2026


### Competing interests

The authors declare that they have no conflict of interest.

### Disclaimer

Copernicus Publications remains neutral with regard to jurisdictional claims made in the text, published maps, institutional affiliations, or any other geographical representation in this paper. While Copernicus Publications makes every effort to include appropriate place names, the final responsibility lies with the authors. Views expressed in the text are those of the authors and do not necessarily reflect the views of the publisher.

### Acknowledgements

The authors thank Ivan Kritskov for terrain logistics and the extraction of cores; Georgy Istigechev, Daria Kuzmina and Nikita Shefer for sampling, extracting and filtering the pore water samples; Egor Istigichev for the extraction of cores, drone photography and ortophotos.

### Financial support

JLR and OSP acknowledge “Ministère de l'Enseignement Supérieur et de la Recherche France" support for the funding of a doctoral scholarship for LPS (ComUE of Toulouse and Occitanie Region ComUE of Toulouse and Occitanie Region (project No. 23003137)). OSP acknowledges partial support from "Agence Nationale de la Recherche France" (project PEACE of PEPR FairCarboN ANR-22-PEXF-0011). SVL and AL acknowledge the support of the State Assignment of the Ministry of Science and Higher Education of the Russian Federation (project No. FSWM-2024-0006).

### Review statement

The review statement will be added by Copernicus Publications listing the handling editor as well as all contributing referees according to their status anonymous or identified.

### References

Åkerman, H. J. and Johansson, M.: Thawing permafrost and thicker active layers in sub-arctic Sweden, Permafrost & Periglacial, 19, 279–292, https://doi.org/10.1002/ppp.626, 2008.

Armstrong, A.: Polygon preservation, Nature Geosci, 5, 91–91, https://doi.org/10.1038/ngeo1398, 2012.

https://doi.org/10.5194/egusphere-2026-3058
Preprint. Discussion started: 24 June 2026


Barczok, M., Smith, C., Kinsman-Costello, L., Patzner, M., Bryce, C., Kappler, A., Singer, D., and Herndon, E.: Iron transformation mediates phosphate retention across a permafrost thaw gradient, Commun Earth Environ, 5, 635, https://doi.org/10.1038/s43247-024-01810-z, 2024.

Baxter, W. B., Smith, J. P., Douglas, T. A., Barbato, R. A., Gallaher, S., and Barker, A. J.: Rare earth elements (REE) as indicators of geochemical processes in permafrost systems of the Arctic Foothills, Northern Alaska, Chemical Geology, 698, 123131, https://doi.org/10.1016/j.chemgeo.2025.123131, 2025.

Bridgham, S. D., Cadillo-Quiroz, H., Keller, J. K., and Zhuang, Q.: Methane emissions from wetlands: biogeochemical, microbial, and modeling perspectives from local to global scales, Global Change Biology, 19, 1325–1346, https://doi.org/10.1111/gcb.12131, 2013.

Byun, E., Rezanezhad, F., Slowinski, S., Lam, C., Bhusal, S., Wright, S., Quinton, W. L., Webster, K. L., and Van Cappellen, P.: Effects of nitrogen and phosphorus amendments on $CO_2$ and $CH_4$ production in peat soils of Scotty Creek, Northwest Territories: potential considerations for wildfire and permafrost thaw impacts on peatland carbon exchanges, SOIL, 11, 309–321, https://doi.org/10.5194/soil-11-309-2025, 2025.

Chapin, F. S., Barsdate, R. J., and Barèl, D.: Phosphorus Cycling in Alaskan Coastal Tundra: A Hypothesis for the Regulation of Nutrient Cycling, Oikos, 31, 189–199, https://doi.org/10.2307/3543562, 1978.

Cory, R. M., Miller, M. P., McKnight, D. M., Guerard, J. J., and Miller, P. L.: Effect of instrument-specific response on the analysis of fulvic acid fluorescence spectra, Limnology and Oceanography: Methods, 8, 67–78, https://doi.org/10.4319/lom.2010.8.67, 2010.

Duddleston, K. N., Kinney, M. A., Kiene, R. P., and Hines, M. E.: Anaerobic microbial biogeochemistry in a northern bog: Acetate as a dominant metabolic end product, Global Biogeochemical Cycles, 16, 11–1, https://doi.org/10.1029/2001GB001402, 2002.

Dumoulin, J.-P., Comby-Zerbino, C., Delqué-Količ, E., Moreau, C., Caffy, I., Hain, S., Perron, M., Thellier, B., Setti, V., Berthier, B., and Beck, L.: Status Report on Sample Preparation Protocols Developed at the LMC14 Laboratory, Saclay, France: From Sample Collection to 14C AMS Measurement, Radiocarbon, 59, 713–726, https://doi.org/10.1017/RDC.2016.116, 2017.

Estop-Aragonés, C., Heffernan, L., Knorr, K.-H., and Olefeldt, D.: Limited Potential for Mineralization of Permafrost Peatland Soil Carbon Following Thermokarst: Evidence From Anoxic Incubation and Priming Experiments, Journal of Geophysical Research: Biogeosciences, 127, e2022JG006910, https://doi.org/10.1029/2022JG006910, 2022.

Feng, X., Nielsen, L. L., and Simpson, M. J.: Responses of soil organic matter and microorganisms to freeze–thaw cycles, Soil Biology and Biochemistry, 39, 2027–2037, https://doi.org/10.1016/j.soilbio.2007.03.003, 2007.

Fewster, R. E., Morris, P. J., Swindles, G. T., Ivanovic, R. F., Treat, C. C., and Jones, M. C.: Holocene vegetation dynamics of circum-Arctic permafrost peatlands, Quaternary Science Reviews, 307, 108055, https://doi.org/10.1016/j.quascirev.2023.108055, 2023.

Fotiev, S.M.: Arctic peatlands of the Yamal-Gydan province of Western Siberia, Earth's Cryosphere, https://doi.org/10.21782/EC1560-7496-2017-5(3-13), 2017.

Fouché, J., Christiansen, C. T., Lafrenière, M. J., Grogan, P., and Lamoureux, S. F.: Canadian permafrost stores large pools of ammonium and optically distinct dissolved organic matter, Nat Commun, 11, 4500, https://doi.org/10.1038/s41467-020-18331-w, 2020.

https://doi.org/10.5194/egusphere-2026-3058
Preprint. Discussion started: 24 June 2026


Frey, K. E. and Smith, L. C.: Amplified carbon release from vast West Siberian peatlands by 2100, Geophysical Research Letters, 32, https://doi.org/10.1029/2004GL022025, 2005.

Frey, K. E., Siegel, D. I., and Smith, L. C.: Geochemistry of west Siberian streams and their potential response to permafrost degradation, Water Resources Research, 43, https://doi.org/10.1029/2006WR004902, 2007.

Fu, Z., Wu, Q., Zhang, W., He, H., and Wang, L.: Water Migration and Segregated Ice Formation in Frozen Ground: Current Advances and Future Perspectives, Frontiers in Earth Science, 10, 2022.

Gandois, L., Tananaev, N. I., Prokushkin, A., Solnyshkin, I., and Teisserenc, R.: Seasonality of DOC Export From a Russian Subarctic Catchment Underlain by Discontinuous Permafrost, Highlighted by High-Frequency Monitoring, Journal of Geophysical Research: Biogeosciences, 126, e2020JG006152, https://doi.org/10.1029/2020JG006152, 2021.

Garcia-Pausas, J. and Paterson, E.: Microbial community abundance and structure are determinants of soil organic matter mineralisation in the presence of labile carbon, Soil Biology and Biochemistry, 43, 1705–1713, https://doi.org/10.1016/j.soilbio.2011.04.016, 2011.

Giblin, A. E., Nadelhoffer, K. J., Shaver, G. R., Laundre, J. A., and McKerrow, A. J.: Biogeochemical Diversity Along a Riverside Toposequence in Arctic Alaska, Ecological Monographs, 61, 415–435, https://doi.org/10.2307/2937049, 1991.

Halaś, A., Lamentowicz, M., Obremska, M., Łuców, D., and Słowiński, M.: Peatland development reconstruction and complex biological responses to permafrost thawing in Western Siberia, Biogeosciences, 22, 4797–4822, https://doi.org/10.5194/bg-22-4797-2025, 2025.

Hamdan, R., El-Rifai, H. M., Cheesman, A. W., Turner, B. L., Reddy, K. R., and Cooper, W. T.: Linking phosphorus sequestration to carbon humification in wetland soils by 31P and 13C NMR spectroscopy, Environ Sci Technol, 46, 4775–4782, https://doi.org/10.1021/es204072k, 2012.

Hamm, A., Schytt Mannerfelt, E., Mohammed, A. A., Painter, S. L., Coon, E. T., and Frampton, A.: Model-based analysis of solute transport and potential carbon mineralization in the active layer of a hillslope underlain by permafrost with seasonal variability and climate change, The Cryosphere, 19, 3693–3724, https://doi.org/10.5194/tc-19-3693-2025, 2025.

Harms, T. K. and Ludwig, S. M.: Retention and removal of nitrogen and phosphorus in saturated soils of arctic hillslopes, Biogeochemistry, 127, 291–304, https://doi.org/10.1007/s10533-016-0181-0, 2016.

Hatté, C., Arnold, M., Dapoigny, A., Daux, V., Delibrias, G., Boisgueheneuc, D. D., Fontugne, M., Gauthier, C., Guillier, M.-T., Jacob, J., Jaudon, M., Kaltnecker, É., Labeyrie, J., Noury, C., Paterne, M., Pierre, M., Phouybanhdyt, B., Poupeau, J.-J., Tannau, J.-F., Thil, F., Tisnérat-Laborde, N., and Valladas, H.: RADIOCARBON DATING ON ECHOMICADAS, LSCE, GIF-SUR-YVETTE, FRANCE: NEW AND UPDATED CHEMICAL PROCEDURES, Radiocarbon, 66, 1166–1181, https://doi.org/10.1017/RDC.2023.46, 2024.

Hayashi, M., Quinton, W. L., Pietroniro, A., and Gibson, J. J.: Hydrologic functions of wetlands in a discontinuous permafrost basin indicated by isotopic and chemical signatures, Journal of Hydrology, 296, 81–97, https://doi.org/10.1016/j.jhydrol.2004.03.020, 2004.

Herrmann, A. and Witter, E.: Sources of C and N contributing to the flush in mineralization upon freeze–thaw cycles in soils, Soil Biology and Biochemistry, 34, 1495–1505, https://doi.org/10.1016/S0038-0717(02)00121-9, 2002.

Hugelius, G., Loisel, J., Chadburn, S., Jackson, R. B., Jones, M., MacDonald, G., Marushchak, M., Olefeldt, D., Packalen, M., Siewert, M. B., Treat, C., Turetsky, M., Voigt, C., and Yu, Z.: Large stocks of peatland carbon and nitrogen are vulnerable to permafrost thaw, Proceedings of the National Academy of Sciences, 117, 20438–20446, https://doi.org/10.1073/pnas.1916387117, 2020.

Ivanova, I. S., Shirokova, L. S., Rols, J.-L., and Pokrovsky, O. S.: Partitioning of Dissolved Organic Carbon, Major Elements, and Trace Metals during Laboratory Freezing of Organic Leachates from Permafrost Peatlands, Applied Sciences, 13, 4856, https://doi.org/10.3390/app13084856, 2023.

Ji, M., Kong, W., Liang, C., Zhou, T., Jia, H., and Dong, X.: Permafrost thawing exhibits a greater influence on bacterial richness and community structure than permafrost age in Arctic permafrost soils, The Cryosphere, 14, 3907–3916, https://doi.org/10.5194/tc-14-3907-2020, 2020.

Kirkwood, J. Adam. H., Roy-Léveillée, P., Mykytczuk, N., Packalen, M., McLaughlin, J., Laframboise, A., and Basiliko, N.: Soil Microbial Community Response to Permafrost Degradation in Palsa Fields of the Hudson Bay Lowlands: Implications for Greenhouse Gas Production in a Warming Climate, Global Biogeochemical Cycles, 35, e2021GB006954, https://doi.org/10.1029/2021GB006954, 2021.

Koch, J. C., Connolly, C. T., Baughman, C., Repasch, M., Best, H., and Hunt, A.: The dominance and growth of shallow groundwater resources in continuous permafrost environments, Proceedings of the National Academy of Sciences, 121, e2317873121, https://doi.org/10.1073/pnas.2317873121, 2024.

Kondratjeva, K. A., Khrutzky, S. F., and Romanovsky, N. N.: Changes in the extent of permafrost during the late quaternary period in the territory of the former Soviet Union, Permafrost & Periglacial, 4, 113–119, https://doi.org/10.1002/ppp.3430040204, 1993.

Kotsyurbenko, O. R., Chin, K.-J., Glagolev, M. V., Stubner, S., Simankova, M. V., Nozhevnikova, A. N., and Conrad, R.: Acetoclastic and hydrogenotrophic methane production and methanogenic populations in an acidic West-Siberian peat bog, Environ Microbiol, 6, 1159–1173, https://doi.org/10.1111/j.1462-2920.2004.00634.x, 2004.

Krickov, I. V., Loiko, S. V., Lim, A. G., Kuzmina, D. M., Istigechev, G. I., Shirokova, L. S., Pupyshev, Y. S., and Pokrovsky, O. S.: Hydrological continuums across climate and permafrost gradients: Spatial patterns of organic carbon, greenhouse gases, and major and trace elements, Water Research, 294, 125507, https://doi.org/10.1016/j.watres.2026.125507, 2026.

Kuzmina, D. M., Lim, A. G., Loiko, S. V., Shefer, N., Shirokova, L. S., Julien, F., Rols, J.-L., and Pokrovsky, O. S.: Dispersed ice of permafrost peatlands represents an important source of labile carboxylic acids, nutrients and metals, Geoderma, 429, 116256, https://doi.org/10.1016/j.geoderma.2022.116256, 2023.

Li, Y., Xue, Y., Roy Chowdhury, T., Graham, D. E., Tringe, S. G., Jansson, J. K., and Taş, N.: Genomic insights into redox-driven microbial processes for carbon decomposition in thawing Arctic soils and permafrost, mSphere, 9, e00259-24, https://doi.org/10.1128/msphere.00259-24, 2024.

Liao, C. and Zhuang, Q.: Quantifying the Role of Snowmelt in Stream Discharge in an Alaskan Watershed: An Analysis Using a Spatially Distributed Surface Hydrology Model, Journal of Geophysical Research: Earth Surface, 122, 2183–2195, https://doi.org/10.1002/2017JF004214, 2017.

Lim, A. G., Loiko, S. V., Kuzmina, D. M., Krickov, I. V., Shirokova, L. S., Kulizhsky, S. P., Vorobyev, S. N., and Pokrovsky, O. S.: Dispersed ground ice of permafrost peatlands: Potential unaccounted carbon, nutrient and metal sources, Chemosphere, 266, 128953, https://doi.org/10.1016/j.chemosphere.2020.128953, 2021.

Lim, A. G., Loiko, S. V., Kuzmina, D. M., Krickov, I. V., Shirokova, L. S., Kulizhsky, S. P., and Pokrovsky, O. S.: Organic carbon, and major and trace elements reside in labile low-molecular form in the ground ice of permafrost peatlands: a case

https://doi.org/10.5194/egusphere-2026-3058
Preprint. Discussion started: 24 June 2026


study of colloids in peat ice of Western Siberia, Environ. Sci.: Processes Impacts, 24, 1443–1459, https://doi.org/10.1039/D1EM00547B, 2022.

Lim, A. G., Manasypov, R. M., Krickov, I. V., Shirokova, L. S., Vorobyev, S. N., and Pokrovsky, O. S.: Greenhouse gases, organic carbon, major and trace elements in ultra-small water bodies (<100 m2) of permafrost peatlands: Assessment across seasons and permafrost gradient, Journal of Hydrology, 660, 133343, https://doi.org/10.1016/j.jhydrol.2025.133343, 2025a.

Lim, A. G., Loiko, S. V., and Pokrovsky, O. S.: Organic matter, nutrients, and colloidal trace elements in pore waters, dispersed ice and aqueous leachates from mineral soils of the permafrost region, Geoderma, 463, 117562, https://doi.org/10.1016/j.geoderma.2025.117562, 2025b.

Lipson, D. A., Haggerty, J. M., Srinivas, A., Raab, T. K., Sathe, S., and Dinsdale, E. A.: Metagenomic Insights into Anaerobic Metabolism along an Arctic Peat Soil Profile, PLOS ONE, 8, e64659, https://doi.org/10.1371/journal.pone.0064659, 2013.

Logan, M. N., Patzner, M. S., VanderRoest, J. P., McGivern, B. B., Srikanthan, N., Simpson, M. J., McKenna, A. M., Wrighton, K. C., Bryce, C., Kappler, A., and Borch, T.: Role of permafrost thaw transitions in biogeochemical nitrogen cycling, Soil & Environmental Health, 3, 100148, https://doi.org/10.1016/j.seh.2025.100148, 2025.

Loiko, S., Raudina, T., Lim, A., Kuzmina, D., Kulizhskiy, S., and Pokrovsky, O.: Microtopography Controls of Carbon and Related Elements Distribution in the West Siberian Frozen Bogs, Geosciences, 9, 291, https://doi.org/10.3390/geosciences9070291, 2019.

Loiko, S., Kuzmina, D., Georgyi, I., Kritskov, I., Lim, A., Klimova, N., Novoselov, A., Konstantinov, A., Novolodskaya, E., and Kulizhskiy, S.: The Transformation of Morphological Properties of Soils Due to the Low Arctic Tundra Shrubification, Vestnik Tomskogo gosudarstvennogo universiteta Biologiya, https://doi.org/10.17223/19988591/59/1, 2023.

Loiko, S. V., Lim, A. G., Kuzmina, D., Krickov, I. V., Manasypov, R. M., Pokrovsky, B. G., Istigechev, G., and Pokrovsky, O. S.: Residual water bodies formed after thermokarst lake drainage in permafrost regions act as hot spots of nutrient and carbon cycling and greenhouse gas emissions, Science of The Total Environment, 1019, 181532, https://doi.org/10.1016/j.scitotenv.2026.181532, 2026.

McKnight, D. M., Boyer, E. W., Westerhoff, P. K., Doran, P. T., Kulbe, T., and Andersen, D. T.: Spectrofluorometric characterization of dissolved organic matter for indication of precursor organic material and aromaticity, Limnology and Oceanography, 46, 38–48, https://doi.org/10.4319/lo.2001.46.1.0038, 2001.

Monteux, S., Weedon, J. T., Blume-Werry, G., Gavazov, K., Jassey, V. E. J., Johansson, M., Keuper, F., Olid, C., and Dorrepaal, E.: Long-term in situ permafrost thaw effects on bacterial communities and potential aerobic respiration, The ISME Journal, 12, 2129–2141, https://doi.org/10.1038/s41396-018-0176-z, 2018.

Moreau, C., Caffy, I., Comby, C., Delqué-Količ, E., Dumoulin, J.-P., Hain, S., Quiles, A., Setti, V., Souprayen, C., Thellier, B., and Vincent, J.: Research and Development of the Artemis 14C AMS Facility: Status Report, Radiocarbon, 55, 331–337, https://doi.org/10.1017/S0033822200057441, 2013.

Morgalev, S. Y., Lim, A. G., Morgaleva, T. G., Morgalev, Y. N., Manasypov, R. M., Kuzmina, D., Shirokova, L. S., Orgogozo, L., Loiko, S. V., and Pokrovsky, O. S.: Fractionation of organic C, nutrients, metals and bacteria in peat porewater and ice after freezing and thawing, Environ Sci Pollut Res, 30, 823–836, https://doi.org/10.1007/s11356-022-22219-1, 2023.

Muster, S., Roth, K., Langer, M., Lange, S., Cresto Aleina, F., Bartsch, A., Morgenstern, A., Grosse, G., Jones, B., Sannel, A. B. K., Sjöberg, Y., Günther, F., Andresen, C., Veremeeva, A., Lindgren, P. R., Bouchard, F., Lara, M. J., Fortier, D., Charbonneau, S., Virtanen, T. A., Hugelius, G., Palmtag, J., Siewert, M. B., Riley, W. J., Koven, C. D., and Boike, J.: PeRL:

https://doi.org/10.5194/egusphere-2026-3058
Preprint. Discussion started: 24 June 2026


a circum-Arctic Permafrost Region Pond and Lake database, Earth System Science Data, 9, 317–348, https://doi.org/10.5194/essd-9-317-2017, 2017.

O'Donnell, J. A., Carey, M. P., Koch, J. C., Baughman, C., Hill, K., Zimmerman, C. E., Sullivan, P. F., Dial, R., Lyons, T., Cooper, D. J., and Poulin, B. A.: Metal mobilization from thawing permafrost to aquatic ecosystems is driving rusting of Arctic streams, Commun Earth Environ, 5, 268, https://doi.org/10.1038/s43247-024-01446-z, 2024.

Olefeldt, D. and Roulet, N. T.: Effects of permafrost and hydrology on the composition and transport of dissolved organic carbon in a subarctic peatland complex, Journal of Geophysical Research: Biogeosciences, 117, https://doi.org/10.1029/2011JG001819, 2012.

Park, Y., Solhtalab, M., Thongsomboon, W., and Aristilde, L.: Strategies of organic phosphorus recycling by soil bacteria: acquisition, metabolism, and regulation, Environ Microbiol Rep, 14, 3–24, https://doi.org/10.1111/1758-2229.13040, 2022.

Pastukhov, A., Knoblauch, C., Beer, C., Ryzhova, I., and Kaverin, D.: Development of permafrost-affected peatlands in the southern limit of the European Russian cryolithozone and their vulnerability to future warming, Science of The Total Environment, 828, 154350, https://doi.org/10.1016/j.scitotenv.2022.154350, 2022.

Pastukhov, A., Kaverin, D., and Loiko, S.: N-Alkanes in Permafrost Peatlands, Plants, 14, https://doi.org/10.3390/plants14030449, 2025.

Pastukhov, A. V., Marchenko-Vagapova, T. I., Kaverin, D. A., Kulizhskii, S. P., Kuznetsov, O. L., and Panov, V. S.: Dynamics of peat plateau near the southern boundary of the East European permafrost zone, Eurasian Soil Sc., 50, 526–538, https://doi.org/10.1134/S1064229317030097, 2017.

Payandi-Rolland, D., Shirokova, L. S., Labonne, F., Bénézeth, P., and Pokrovsky, O. S.: Impact of freeze-thaw cycles on organic carbon and metals in waters of permafrost peatlands, Chemosphere, 279, 130510, https://doi.org/10.1016/j.chemosphere.2021.130510, 2021.

Pedersen, E. P., Elberling, B., and Michelsen, A.: Upslope release—Downslope receipt? Multi-year plant uptake of permafrost-released nitrogen along an arctic hillslope, Journal of Ecology, 110, 1896–1912, https://doi.org/10.1111/1365-2745.13925, 2022.

Pokrovsky, O. S., Karlsson, J., and Giesler, R.: Freeze-thaw cycles of Arctic thaw ponds remove colloidal metals and generate low-molecular-weight organic matter, Biogeochemistry, 137, 321–336, https://doi.org/10.1007/s10533-018-0421-6, 2018.

Pokrovsky, O. S., Manasypov, R. M., Kopysov, S. G., Krickov, I. V., Shirokova, L. S., Loiko, S. V., Lim, A. G., Kolesnichenko, L. G., Vorobyev, S. N., and Kirpotin, S. N.: Impact of Permafrost Thaw and Climate Warming on Riverine Export Fluxes of Carbon, Nutrients and Metals in Western Siberia, Water, 12, 1817, https://doi.org/10.3390/w12061817, 2020.

Poulin, B. A., Ryan, J. N., and Aiken, G. R.: Effects of Iron on Optical Properties of Dissolved Organic Matter, Environ. Sci. Technol., 48, 10098–10106, https://doi.org/10.1021/es502670r, 2014.

Qin, S., Wang, G., Zhang, D., and Yang, Y.: Increased microbial carbon use efficiency upon abrupt permafrost thaw, Proc Natl Acad Sci U S A, 122, e2419206122, https://doi.org/10.1073/pnas.2419206122, 2025.

Ramsey, C. B.: Development of the Radiocarbon Calibration Program, Radiocarbon, 43, 355–363, https://doi.org/10.1017/S0033822200038212, 2001.

Ramsey, C. B.: Deposition models for chronological records, Quaternary Science Reviews, 27, 42–60, https://doi.org/10.1016/j.quascirev.2007.01.019, 2008.

Ramsey, C. B. and Lee, S.: Recent and Planned Developments of the Program OxCal, Radiocarbon, 55, 720–730, https://doi.org/10.1017/S0033822200057878, 2013.

Rantanen, M., Karpechko, A. Y., Lipponen, A., Nordling, K., Hyvärinen, O., Ruosteenoja, K., Vihma, T., and Laaksonen, A.: The Arctic has warmed nearly four times faster than the globe since 1979, Commun Earth Environ, 3, 168, https://doi.org/10.1038/s43247-022-00498-3, 2022.

Raudina, T., Loiko, S., Lim, A., Kritskov, I., Shirokova, L., Georgyi, I., Kuzmina, D., Kulizhskiy, S., Vorobyev, S., and Pokrovsky, O.: Dissolved organic carbon, major and trace element in peat pore water of sporadic, discontinuous and continuous permafrost zone of Western Siberia, Biogeosciences Discussions, 1–30, https://doi.org/10.5194/bg-2017-24, 2017a.

Raudina, T. V., Loiko, S. V., Lim, A. G., Krickov, I. V., Shirokova, L. S., Istigechev, G. I., Kuzmina, D. M., Kulizhsky, S. P., Vorobyev, S. N., and Pokrovsky, O. S.: Dissolved organic carbon and major and trace elements in peat porewater of sporadic, discontinuous, and continuous permafrost zones of western Siberia, Biogeosciences, 14, 3561–3584, https://doi.org/10.5194/bg-14-3561-2017, 2017b.

Raudina, T. V., Loiko, S. V., Lim, A., Manasypov, R. M., Shirokova, L. S., Istigechev, G. I., Kuzmina, D. M., Kulizhsky, S. P., Vorobyev, S. N., and Pokrovsky, O. S.: Permafrost thaw and climate warming may decrease the CO2, carbon, and metal concentration in peat soil waters of the Western Siberia Lowland, Science of The Total Environment, 634, 1004–1023, https://doi.org/10.1016/j.scitotenv.2018.04.059, 2018.

Raudina, T. V., Loiko, S. V., Istigechev, G. I., Kulizhskiy, S. P., Orgogozo, L., and Pokrovsky, O. S.: Contrasting soil temperature regimes in peatlands of the discontinuous permafrost zone (Western Siberia), Geoderma, 457, 117294, https://doi.org/10.1016/j.geoderma.2025.117294, 2025.

Reddy, K. R. and DeLaune, R. D.: Biogeochemistry of Wetlands: Science and Applications, CRC Press, Boca Raton, 800 pp., https://doi.org/10.1201/9780203491454, 2008.

Reimer, P. J., Austin, W. E. N., Bard, E., Bayliss, A., Blackwell, P. G., Ramsey, C. B., Butzin, M., Cheng, H., Edwards, R. L., Friedrich, M., Grootes, P. M., Guilderson, T. P., Hajdas, I., Heaton, T. J., Hogg, A. G., Hughen, K. A., Kromer, B., Manning, S. W., Muscheler, R., Palmer, J. G., Pearson, C., Plicht, J. van der, Reimer, R. W., Richards, D. A., Scott, E. M., Southon, J. R., Turney, C. S. M., Wacker, L., Adolphi, F., Büntgen, U., Capano, M., Fahrni, S. M., Fogtmann-Schulz, A., Friedrich, R., Köhler, P., Kudsk, S., Miyake, F., Olsen, J., Reinig, F., Sakamoto, M., Sookdeo, A., and Talamo, S.: The IntCal20 Northern Hemisphere Radiocarbon Age Calibration Curve (0–55 cal kBP), Radiocarbon, 62, 725–757, https://doi.org/10.1017/RDC.2020.41, 2020.

Roehm, C. L., Giesler, R., and Karlsson, J.: Bioavailability of terrestrial organic carbon to lake bacteria: The case of a degrading subarctic permafrost mire complex, Journal of Geophysical Research: Biogeosciences, 114, https://doi.org/10.1029/2008JG000863, 2009.

Romanovsky, V. E., Drozdov, D. S., Oberman, N. G., Malkova, G. V., Kholodov, A. L., Marchenko, S. S., Moskalenko, N. G., Sergeev, D. O., Ukraintseva, N. G., Abramov, A. A., Gilichinsky, D. A., and Vasiliev, A. A.: Thermal state of permafrost in Russia, Permafrost and Periglacial Processes, 21, 136–155, https://doi.org/10.1002/ppp.683, 2010.

Rooney, E. C., VanderJeugdt, E., Avasarala, S., Miah, I., Berens, M. J., Kinsman-Costello, L., Weintraub, M. N., and Herndon, E. M.: Decoupling of redox processes from soil saturation in Arctic tundra, Commun Earth Environ, 5, 746, https://doi.org/10.1038/s43247-024-01927-1, 2024.

Schmidt, O., Hink, L., Horn, M. A., and Drake, H. L.: Peat: home to novel syntrophic species that feed acetate- and hydrogen-scavenging methanogens, ISME J, 10, 1954–1966, https://doi.org/10.1038/ismej.2015.256, 2016.

Sheng, Y., Smith, L. C., MacDonald, G. M., Kremenetski, K. V., Frey, K. E., Velichko, A. A., Lee, M., Beilman, D. W., and Dubinin, P.: A high-resolution GIS-based inventory of the west Siberian peat carbon pool, Global Biogeochemical Cycles, 18, https://doi.org/10.1029/2003GB002190, 2004.

Sherstyukov, A. B. and Sherstyukov, B. G.: Spatial features and new trends in thermal conditions of soil and depth of its seasonal thawing in the permafrost zone, Russ. Meteorol. Hydrol., 40, 73–78, https://doi.org/10.3103/S1068373915020016, 2015.

Thil, F., Tisnérat-Laborde, N., Hatté, C., Kader, E., Noury, C., Paterne, M., Phouybanhdyt, B., and Wacker, L.: 14C MICROSAMPLE ANALYSIS WITH ECHoMICADAS FACILITIES: CURRENT STATE OF PLAY, Radiocarbon, 66, 1379–1394, https://doi.org/10.1017/RDC.2024.76, 2024.

Tikhonravova, Y., Kuznetsova, A., Slagoda, E., and Koroleva, E.: Holocene permafrost peatland evolution in drained lake basins on the Pur-Taz Interfluve, North-Western Siberia, Quaternary International, 669, 32–42, https://doi.org/10.1016/j.quaint.2023.07.005, 2023.

Vasil'chuk, Y. and Vasil'chuk, A.: Thick polygonal peatlands in continuous permafrost of West Siberia, Earth's Cryosphere, 20, 3–15, https://doi.org/10.21782/KZ1560-7496-2016-4(3-15), 2016.

Vasil'chuk, Y., Budantseva, N., Vasil'chuk, A., Ginzburg, A., and Tokarev, I.: AMS radiocarbon age and stable oxygen and hydrogen isotopes ratio of Holocene ice wedges of the Pur-Taz interfluve, Radiocarbon, 1–13, https://doi.org/10.1017/RDC.2026.10206, 2026.

Vasiliev, A. A., Drozdov, D. S., Gravis, A. G., Malkova, G. V., Nyland, K. E., and Streletskiy, D. A.: Permafrost degradation in the Western Russian Arctic, Environ. Res. Lett., 15, 045001, https://doi.org/10.1088/1748-9326/ab6f12, 2020.

Voggenreiter, E., ThomasArrigo, L., Bottaro, M., Kilian, J., Straub, D., Ring-Hrubesh, F., Bryce, C., Stahl, M., Kappler, A., and Joshi, P.: Suppression of Methanogenesis by Microbial Reduction of Iron-Organic Carbon Associations in Fully Thawed Permafrost Soil, Journal of Geophysical Research: Biogeosciences, 130, e2024JG008650, https://doi.org/10.1029/2024JG008650, 2025.

Vonk, J. E., Tank, S. E., Mann, P. J., Spencer, R. G. M., Treat, C. C., Striegl, R. G., Abbott, B. W., and Wickland, K. P.: Biodegradability of dissolved organic carbon in permafrost soils and aquatic systems: a meta-analysis, Biogeosciences, 12, 6915–6930, https://doi.org/10.5194/bg-12-6915-2015, 2015.

Walz, J., Knoblauch, C., Böhme, L., and Pfeiffer, E.-M.: Regulation of soil organic matter decomposition in permafrost-affected Siberian tundra soils - Impact of oxygen availability, freezing and thawing, temperature, and labile organic matter, Soil Biology and Biochemistry, 110, 34–43, https://doi.org/10.1016/j.soilbio.2017.03.001, 2017.

Wang, H.-Y., Yu, Z.-G., Zhou, F.-W., Hernandez, J.-C., Grandjean, A., Biester, H., Xiao, K.-Q., and Knorr, K.-H.: Microbial communities and functions are structured by vertical geochemical zones in a northern peatland, Science of The Total Environment, 950, 175273, https://doi.org/10.1016/j.scitotenv.2024.175273, 2024.

Weishaar, J. L., Aiken, G. R., Bergamaschi, B. A., Fram, M. S., Fujii, R., and Mopper, K.: Evaluation of specific ultraviolet absorbance as an indicator of the chemical composition and reactivity of dissolved organic carbon, Environ Sci Technol, 37, 4702–4708, https://doi.org/10.1021/es030360x, 2003.

https://doi.org/10.5194/egusphere-2026-3058
Preprint. Discussion started: 24 June 2026


Woo, M.: Active Layer Dynamics, in: Permafrost Hydrology, edited by: Woo, M., Springer, Berlin, Heidelberg, 163–227, https://doi.org/10.1007/978-3-642-23462-0_5, 2012.

Wright, N., Hayashi, M., and Quinton, W. L.: Spatial and temporal variations in active layer thawing and their implication on runoff generation in peat-covered permafrost terrain, Water Resources Research, 45, https://doi.org/10.1029/2008WR006880, 2009.

Wu, F. and Tanoue, E.: Isolation and partial characterization of dissolved copper-complexing ligands in streamwaters, Environ Sci Technol, 35, 3646–3652, https://doi.org/10.1021/es0019023, 2001.

Xue, H., Oestreich, A., Kistler, D., and Sigg, L.: Free cupric ion concentrations and Cu complexation in selected Swiss lakes and rivers, Aquatic Science, 58, 69–87, https://doi.org/10.1007/BF00877641, 1996.

Yan, J., Sheng, L., Yu, X., Ding, S., Min, Y., Shen, H., and Zou, Y.: Freeze-thaw carry-over effect promotes decomposition of recalcitrant carbon in peatlands by nitrogen limitation, Geoderma, 454, 117182, https://doi.org/10.1016/j.geoderma.2025.117182, 2025.

Zhang, Z., Jiang, L., Chen, M., Li, J., Zhang, L., Zhang, J., and Liao, N.: Release and transformation of phosphorus in sediment following seasonal freezing-thawing cycles, Journal of Contaminant Hydrology, 247, 103978, https://doi.org/10.1016/j.jconhyd.2022.103978, 2022.